Radio controlled autogiro aerodynamic design

Working Paper · April 2016

DOI: 10.13140/RG.2.1.4976.6807

1 author:

Bruno Zilli
C.M.P. OFFICINE MECCANICHE S.r.l. - Udine
12 PUBLICATIONS **0** CITATIONS

R.C.A. AERODYNAMIC DESIGN

abstract: a r.c. model autogyro (R.C.A.) aerodynamic design
attached docs: mathematical models, calculations and drawings
author: Ing. Bruno Zilli – bruno.zilli@libero.it
release: **REV00**

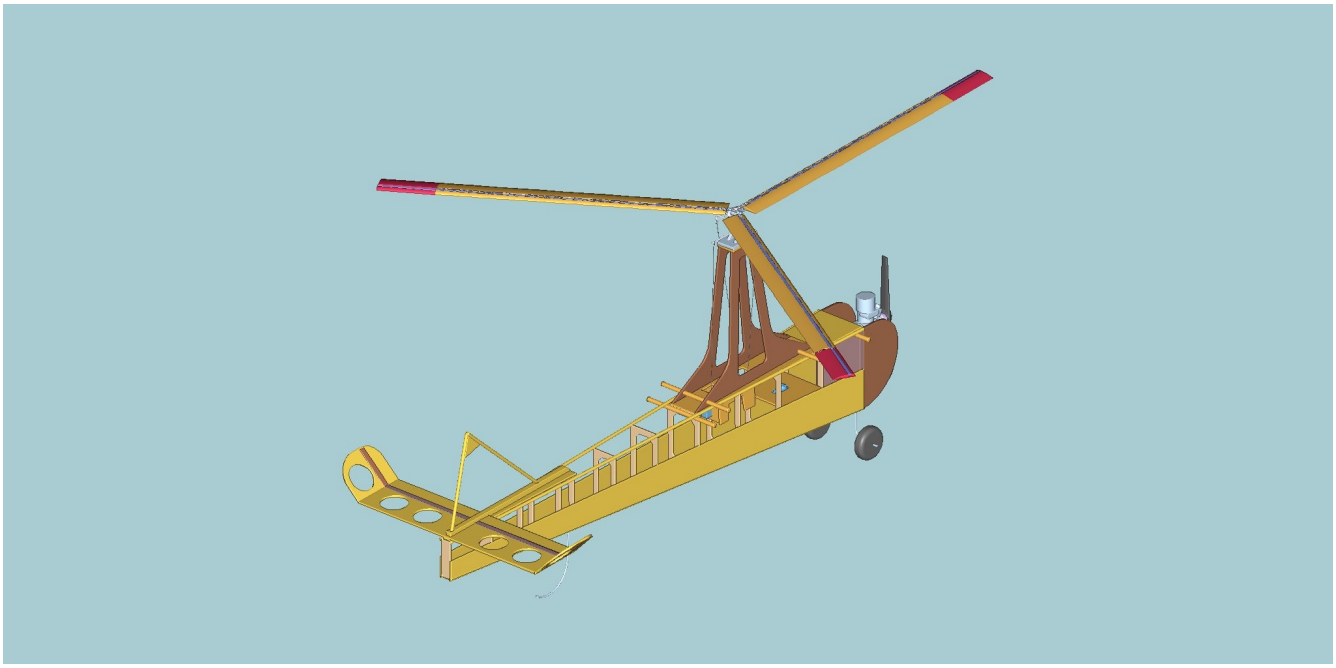

« Il y a un édifice immense dont j'ai posé le fondement de mes mains : il était solide et simple, tous les hommes pouvaient y entrer en sûreté ; ils ont voulu y ajouter les ornements les plus bizarres, les plus grossiers, et les plus inutiles ; le bâtiment tombe en ruine de tous les côtés ; les hommes en prennent les pierres, et se les jettent à la tête ; je leur crie : Arrêtez, écartez ces décombres funestes qui sont votre ouvrage, et demeurez avec moi en paix dans l'édifice inébranlable qui est le mien. »

(Voltaire – Traité sur la tolérance)

Contents

Appendix

1.Summary

This document contains some useful information and mathematical models and methods for a r.c. model autogyro design. The task is doing a simple and useful paper for radio controlled autogyro design. **The author strictly warns to use this paper and all its contents for r.c. models only.**
In chapter #2 I discuss the characteristic lay-out for a classic forward traction autogyro. So we can plot a generic drawing of autogyro.
In chapter #3 there is an explanation taken essentially from Leishman and Glauert about the autogyro aerodynamics, with some drawings to easily understand this machine flying principles and problems.
In chapter #4 I discuss the typical parameters of disc specific load and power consumption, so we can decide the disc size, the solidity and the engine size.
In chapter #5 there are some mathematical model blades with a classic approach from the structural matrix theory.
In chapter #6 computational analysis of the autogyro blade was performed by software made by the author working under Scilab-Inria.
In chapter #7 is analyzed in detail a typical flexible hub.
In chapter #8 is analyzed the good effect of a delta-hub rotor.
In chapter #9 there's an analysis on the rotor flutter stability.
In chapter #10 there is an investigation on vehicle stability during flight.
In chapter #11 there's a synthesis of ideas, in order to do a consistent design.
Conclusions are in chapter #12 and some notes in the appendix, bibliography A1, software list A2 and some notes about final flying tests A3.
In A4 there are some notes about the author and general information about this work.

Chapters have been written in detail increasing, and also as stand-alone parts. The aim of this work is to give suggestions to all the modeler friends of mine, who want to design and build their own gyros.

Also reading only the chapter #2 should be enough to construct something good without having a ph.d. in mathematics. If somebody is crazy for science, there are a lot of things in the following chapters of intrest. My intentions have been to collect, synthesize and making available for modelers, all the lost (*intentionally hidden?*) information for understanding and building-up with conscience a good gyro model.

The choice of English has been done intentionally for the best comprehension and diffusion of this paper.

Special thanks to Doctor Josef Trchalik – Univesity Of Glasgow, who supported and encouraged this work.

2.Geometric Lay-Out

In this chapter there is a collection of general information on the classic geometry proportions of a r.c. tractor style no-winged model autogyro.
In simple words, the autogyro depends on an initial angle of attack of the rotor. While it remains positive, an average of 10°, lifting force is produced by blades lifting foils. Note that this kind of profile (for an autogyro is typically a NACA 8H12), is different from the helicopter blades symmetric profile. In order to control the direction and the lift of our autogyro, we tilt the rotor disk by servos action (direct servo controlled autogyro). With the elevator and rudder, we can perform the same action as well togheter with the disk action (tail controlled autogyro).
All the values and the parameters reported here below offer a good beginning in general. We consider the drawing #2.1 here below.

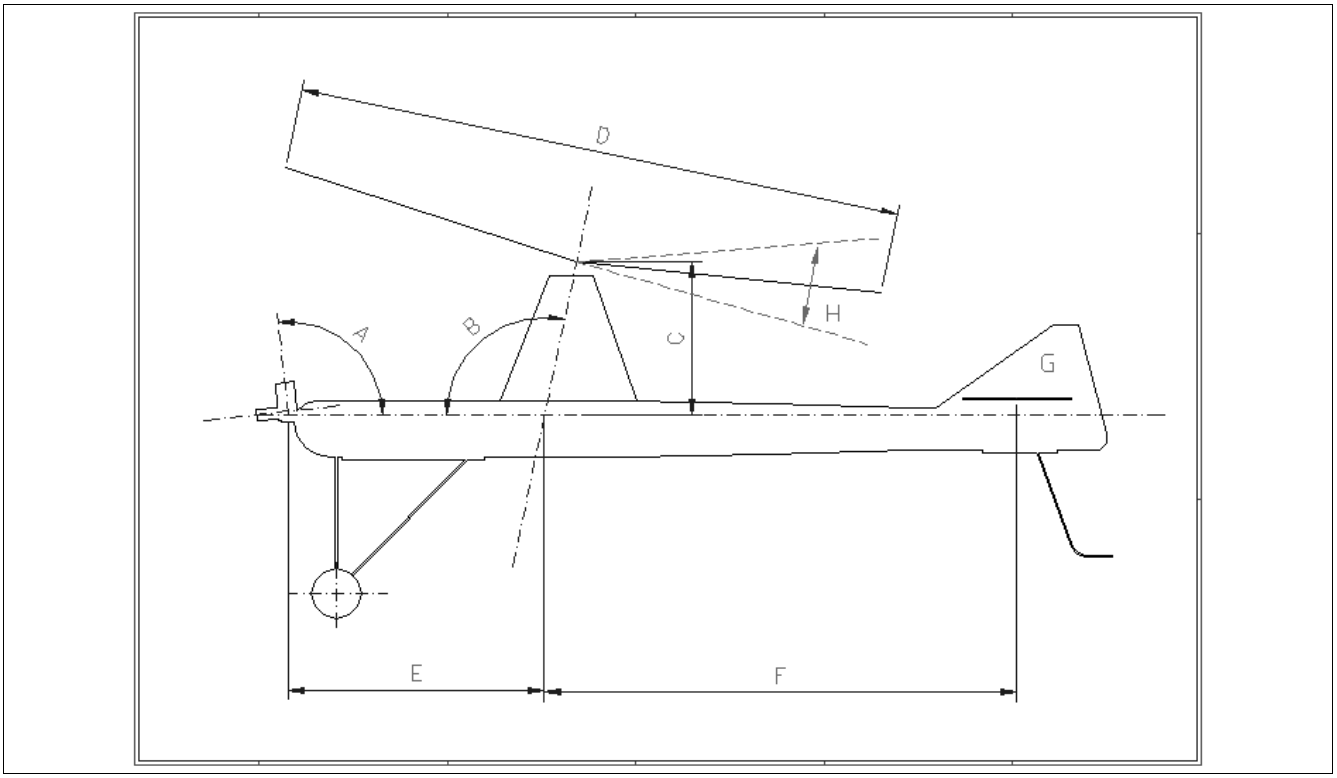

-2.1-

A – Engine down thrust angle – 5° (typically from 3° to 8°)

This angle is necessary to counterbalance the rotor drag which is high above the horizontal centerline and center of gravity.
A higher amount of A, e.g. 10° or more is most probably due to an excessive disk height. This causes an increasing of the drag force that needs to be counterbalanced by a higher angle A. If the rotor disk is placed lower, it reduces the angle A to 5°- 8°.

B – Mast angle – 10° (typically from 6° to 14°)

It seems that B depends on the stabilizer installed, size, position and profile, as well by A angle and the C.G. position. With a trusting tail, angle B increases. With a neutral profile stabilizer, angle B decreases. Sometimes it needs a slight correction of the neutral mast angle. It depends also from the Engine down thrust angle. The more the down trust angle, the more the mast angle results.

C – Rotor disk height

Roughly same as E, but not more than E. Somepeople says 25% more than E. One finding is that the higher the rotor (vertically), the more stable the model, however the less handling, it may possibly resist a turn. On the other hand, the lower the rotor height, the more maneuverable the model is. Generally speaking, a model with a very high rotor position is requires coordinate rudder assistance to complete a turn. With totally direct control fins models (without rudder and elevator), the rotor height is more critical for reaching a coordinated flight, therefore these kind of models are more difficult to design and fly.
The main advantage of a direct control model (tilting rotor) is more controllable over all its speed range. It can also be controlled down to zero forward airspeed, compared to a rudder/elevator and no tilting rotor.

D – Rotor disk diameter

It is enough to obtain a disk specific load of less than 15 g/dm^2 (5 ozs/ft^2). With specific loads more than 15 g/dm^2, they will experience problems with hovering, a longer ground take off distance, and/or be more difficult to hand launch. Better models have 10-15 g/dm^2 as specific disk loads.
To find and to predict the model flight, we discuss the typical parameters in chapter 4 to size the engine. Important note: a rotor diameter increasing causes also a drag increasing, so the right size of the rotor is important and shouldn't has to be changed out of the given specific disk load range.

Rotor disk solidity

In simple word it's the number of blades we're using for our rotor. Three or four blades is the working solution. Actually the number of blades isn't critical for model performance. Notice that the rpm decreases with the more blades we add.
The model autogyro could work with only one well balanced blade, but it isn't a good solution because of the higher launch spinning rotational speed. Usually there are two or more. Three is a very good design, four is finer for bigger models and for rotor efficiency (lift). Four blades seem to add some more stability to the model (because of a little bit more rotor inertia).
A good idea would be to make some extra blades more when we're building our model, because sooner or later we're going to have to replace them.

Rotor blade aspect ratio

10:1 is a good design. A good range is from 8:1 to 12:1. The blade thickness should be less than 16% of the chord-width. Blades with more than 16% are difficult to spin at the take off.
The best thickness should be form 13% than 16% of the chord length.
It's better to have a narrow leading edge radius, with a thin trailing edge. For model gyros clark Y-W-K bottom flattened have been used with success.
A good way is the bottom flattened clark-YS with a slightly reflexed trailing edge. This is done to prevent the bending down (tuck-under) of the leading edge.
The SG6042 is a very good airfoil and so is the well known NACA 8H12 universally known as the autogyro profile.

E – Prop to mast

Roughly equal to C, to be kept short just to balance the model forward to the rotor shaft. To achive a stable model the rotor is normally placed higher than the length of the nose. If we're dealing with with a direct controlled rotor to control the model, a longer nose makes turning a model more difficult.
The nose length C has to be kept as short as possible also for weight balancing problems.

Center of gravity (C.G.)

The model needs to be balanced just forward of the rotor shaft (as winged models is the stability margin) and above the fuselage line. Commonly happens that the C.G. is a point where it's difficult to hold the model. To find out if the model is balanced well or not, we hold the model from the rotor shaft and we observe the nose down aptitude from a horizontal line. This hang angle has to be from 5° to 10°. The greater this angle, the heavier the model flight but stable is more. Important: models with the C.G. under the rotor will be extremely sensitive in both pitch and roll. A tractor style autogyro with a small or no hang angle won't assume a nose down glide position with engine failure and thus will be virtually uncontrollable.

F- Rotor to tail distance

Normally, F is double the distance of E. Unnecessary tail extension causes problems as stated above for a nose extension. Once the rotor is sized, the tail fin will be placed just aft of the rotor max radius (more than 1/2” or 1”). If the fuselage is thin enough to flex during landings, additional clearance may be needed.

G – Vertical fin area and horizontal stabilizer area

It's approximately 2.0 to 3.5% of the rotor disk area and approximately 45 to 55% of the horizontal stabilizer area. This parameter will vary greatly depending on the particular design. The tail feathers need to be kept close (but allow at least 1/2 to 1”) blade tip clearance.
Extending the tail well aft of the model may increase its stability, however decreases its aptitude to complete a coordinated turn without the need for lots of rudder assistance.
Horizontal stabilizer area is approximately 5 to 8% of the rotor disk area. Normally if the rotor is servo controlled, and elevator plus rudder control is not used, the tail can be slightly smaller in size.

These topics (vertical fin and stab area with stability) will be discussed in detail in chapters #10.

H – Rotor pitch control limits - ± 8°

Roll lateral control limits - ± 7°

These values are applied to direct controlled rotor models, that seem to be more sensitive in roll than in pitch. Due to the specific autogyro design, an extra lift could be found on the left part of the rotor (watching model from behind), for a c.c.w. rotor.
It means that we must provide some more servo excursion for left turning, this before initial flight tests.
This topic (lifting asymmetry) will be discussed in detail in chapter #3.

Engine power

The generally acceptable requirement is a thrust to be equal at least to half of the weight of the model. A thrust of 75% the model weight would be better. Ratio 1:1 isn't necessary.

3. Autogyro General Theory

Dimensions of blades

B = Number of blades.
θ(r) = aerofoil blade section angle of pitch.
R = extreme radius.
A = Disk rotor area.
r = radius of the blade element.
c(r) = chord of blade element.
h(r) = ordinate from base line
χ(r) = slope of blade element
W1 = g*mass (weight) of one blade, g is 9.81 m/s^2.
G1 = g*mass (weight) moment to hinge.
I_1,J_1 = moment of inertia and product of inertia.

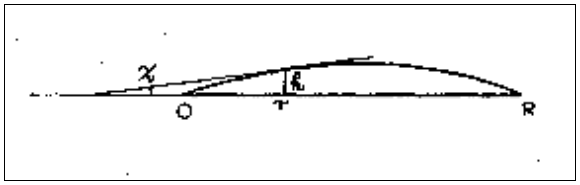

Motion of blades

Ω = angular velocity of shaft.
ψ = angular position of blade.
β = angular rotation of blade around its hinge.
$\beta = \beta_0 - \beta_1 \cos(\Psi - \Psi_1)$.

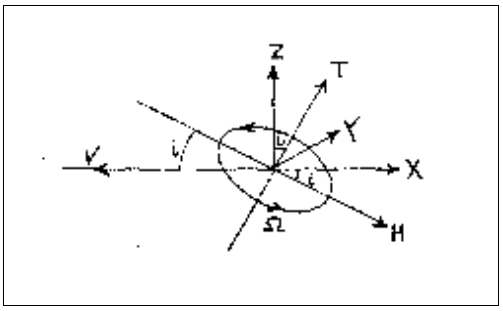

General motion

i = angle of incidence of autogyro - disk rotor theory (mast angle if horizontal flight).
α_{HP} = rotor hub-plane angle with relative wind in detailed rotor theory.
α_{TPP} = rotor tip-path-plane angle with relative wind in detailed rotor theory.
V = forward speed.
v_i = axial induced velocity.
v_h = hovering induced velocity.
V^* = resultant of V and v.
u = axial velocity through disc.
V_c = climbing velocity.
U = resultant velocity relative to blade element.
Φ = slope of U.

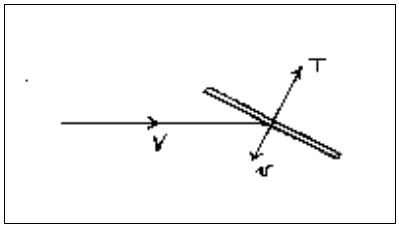

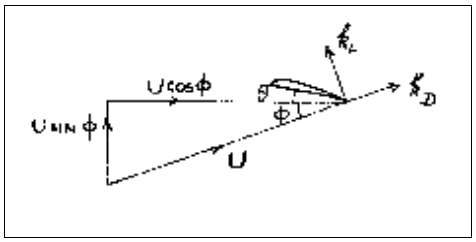

Forces

W = total weight.

$w = \frac{W}{\pi R^2}$ specific disc load.

T = thrust.
D = drag.
Y = lateral force.
L = lift.
Q = torque.

Coefficients

$CT = \frac{T}{\pi R^2 \rho \Omega^2 R^2}$ thrust coefficient

$k_D = \frac{D}{\pi R^2 \rho V^2}$

k_L, k_D = lift and drag coefficients of blade element in disk rotor theory.
Cd and Cl = lift and drag coefficients of blade element in the detailed rotor theory.

δ = mean profile drag coefficient.

$\sigma = \frac{Bc}{\pi R}$ solidity.

$\mu = \frac{V\cos(\alpha)}{\Omega R}$ rotor advance ratio

$\chi = \frac{u}{\Omega R}$

$\zeta = \frac{8}{3}\theta^2 + \frac{17}{2}\theta\chi + \frac{15}{2}\chi^2$

ξ, η_1, η_2 = coefficients of the blade curvature.
ε, μ_1, μ_2 = coefficients of the blade density.

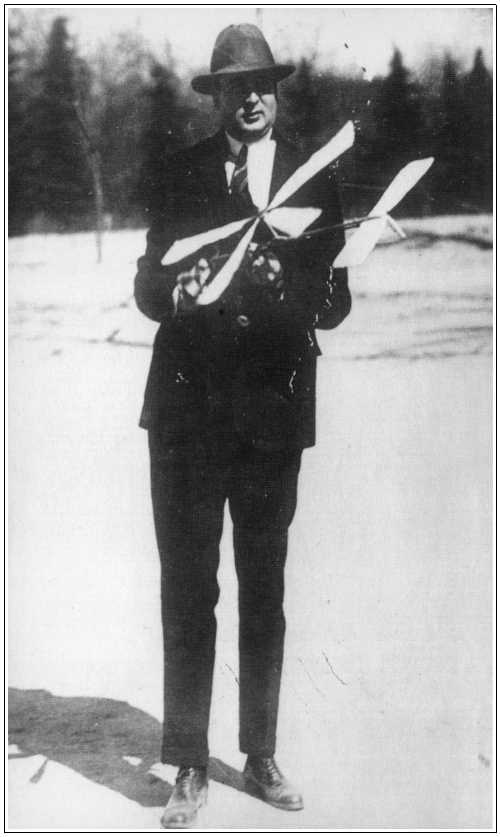

Ing. Juan De La Cierva stated:"..*the wings of such an aircraft should be moving in relation to the fuselage. The only mechanism able to satisfy this requirement is a circular motion and, moreover, in order to give adequate security to the aforementioned requirement it must be independent of the engine. It was thus necessary that these rotary wings were free-spinning and unpowered...*".

The autogyro rotor always operates in the auto rotative working state, where the power to turn the rotor comes from a relative flow that is directed upward through the rotor disk. An autogyro rotor has got a low disk loading (T/A). This means a small upward flow normal to the tip-path plane is necessary to produce auto rotation. Therefore. In straight-and-level forward flight the rotor needs to operate only with a slight positive angle of attack (i). The loss of engine is never a problem on an autogyro, because the rotor is always in the auto rotative state. The machine will descend safely.
Auto rotation can be defined as a self sustained rotation of the rotor without the application of any torque Q = 0. Under this condition the air stream gives the rotor the necessary energy to rotate. This air stream is directed upward through the rotor.

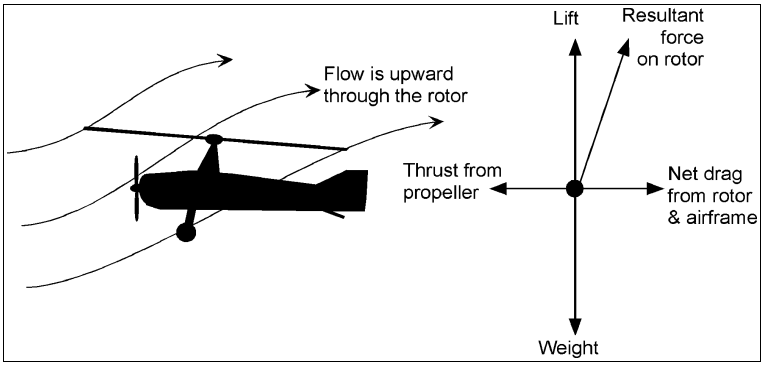

The use of an integral method affords considerable mathematical simplification, but means only what happens before and after the rotor disk. It gives no information on what happens at the blade level.
If Qh is the torque needed for a rotor in hovering state, V_c the climbing velocity, vh the induced velocity in hovering state, v_i the induced velocity, it is:

$$\frac{Q}{Qh}=\frac{Vc}{vh}+\frac{vi}{vh}$$

Glauert gave a first measure of vi, $vi=\frac{T}{2\pi R^2 \rho V}$ if i (incidence) and T are small.

$\frac{Vc}{vh}$ is proportional to the rotor potential energy change and $\frac{vi}{vh}$ is proportional to the aerodynamic losses.

The solution for $\frac{vi}{vh}$ depends on the operating state. For a climb the solution is:

$\frac{vi}{vh}=-(\frac{Vc}{2vh})+\sqrt{(\frac{Vc}{2vh})^2-1}$ and for descending flight $\frac{vi}{vh}=-(\frac{Vc}{2vh})-\sqrt{(\frac{Vc}{2vh})^2-1}$

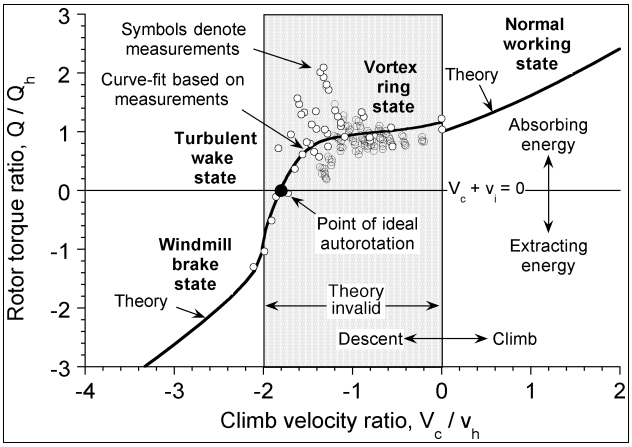

the latter equation being valid only for $\frac{Vc}{vh}\leqslant -2$.

The result for $\frac{Q}{Qh}$ are reported in fig. 3-1 in the form of a non dimensional curve.

Notice that there is no exact theory to describe the flow in the region $-2\leqslant\frac{Vc}{vh}\leqslant 0$ (which includes the auto rotative state), and the nature of the curve is obtained empirically. It's important that in a descent at least above a certain rate $\frac{Vc}{vh}$, the rotor is driven by air.

There is a value of $\frac{Vc}{vh}$ for which no net torque is required at the rotor, that is, when the curve crosses the auto rotational line Vc + vi = 0. So that, $P=Q\Omega=T(Vc+vi)=0$ or $\frac{Q}{Qh}$ = 0.

This condition is usually called ideal auto rotation, (ideal) although because the nature of this curve is empirical, it includes non ideal losses.

This condition occurs when the rotor is descending vertically at $\frac{Vc}{vh}\approx -1.75$.

Caused by the profile losses, the real auto rotation in vertical flight occurs at slightly higher rate than this. In an actual auto rotation condition this is:

$$Q=(\frac{T}{\Omega})(Vc+vi)+Q0=0$$

It will be apparent then that when in a stable “gliding auto rotation” with a constant airspeed and constant rotor rpm there is an energy balance where the decrease in potential energy of the rotor TVc just balances the sum of the induced and the profile losses of the rotor.
De La Cierva explored this idea at the beginning of his experiences with autogyros.

So we've got: $\frac{Vc}{vh}=\frac{-vi}{vh}-\frac{Q0\Omega}{Tvh}$

The term second on the right of this last equation varies form 0.04 to 0.09, depending on the rotor efficiency. This is the profile drag of the rotor.

Profile drag depends on rotor solidity σ = $\frac{Bc}{\pi R}$ and the drag of the airfoil section used on the blades.

So we can decide that this term $\frac{Q0\Omega}{Tvh}$ of extra rate of descent required to overcome profile losses is relatively small than the first one. So have that a real vertical auto rotation of the rotor will occur for values $-1.85 \leqslant \frac{Vc}{vh} \leqslant -1.8$.

So we've for 1.85: $Vd \approx 1.85\sqrt{(\frac{T}{2\rho A})}$ at sea level.

Glauert also proposed the idea that an autogyro works like having a circular wing at a certain angle of incidence i (disk theory).

If we don't consider the periodic terms (due to the rotor swinging), we've from Glauert:

$W \approx T = B\,c\,\Omega^2 R^3(\theta + \frac{3}{2}\chi) = \frac{1}{3}kL\,B\,c\,\Omega^2 R^3$ where $\chi = \sqrt{(\theta + \frac{3}{2}\delta - \theta)}$ under the assumption that

$k_D = \delta$ or $CT = \frac{1}{3}\sigma kL$ $kL = 3(\theta + \Phi) = 3(\theta + \frac{3}{2}\chi), (\theta + \Phi) \leqslant 0.15$ and

The following table gives k_L for a suitable range of values of θ and δ (from Glauert).

θ =	0°	2°	4°	6°
δ = 0	0	0·105	0·210	0·315
0·003	0·101	0·166	0·250	0·345
0·006	0·142	0·204	0·282	0·370
0·010	0·184	0·244	0·317	0·400
0·015	0·225	0·284	0·353	0·432

From Leishman- Also of interest is the auto rotational rate of descent vs the rotor disk angle of attack. Auto rotation is also possible in level flight with propulsion to drive the auto giro forward. All that is required is that the rotor disk be held at a sufficient angle of attack such that the component of the relative wind upwards through the disk causes the rotor to auto rotate. In the words of Juan de la Cierva, “It makes no difference at what angle the Auto giro is climbing or flying. The blades are always gliding toward a point a little below the focus of forward flight. Its is impossible, therefore, for auto rotation to stop while the machine is in movement.”

Reproduced from Leishman

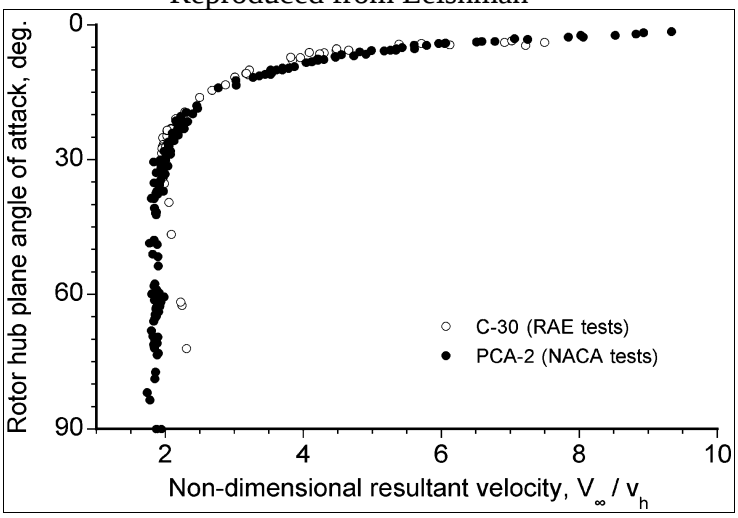

The results in the opposite figure show the measured hub plane angle of attack as a function of the resultant non dimensional velocity of the aircraft.
In a pure vertical descent it is apparent that the tip-path plane and hub plane angles of attack are both 90 deg. (The resultant wind is perpendicular to the disk.) As forward speed builds, the hub plane needs to make a progressively smaller angle to the relative wind to enable auto rotation until at higher speeds the rotor must be held only at a shallow angle to produce enough lift in the auto rotational state.

The rotor tip-path plane angle is also inclined back, but is not equal to the hub plane angle of attack because of blade flapping (see next figure and also later discussion). The natural tendency to produce longitudinal flapping β1c with forward speed increases the component of velocity upward through the disk, which means the hub plane angle is always small in forward flight. The tip-path plane has a positive angle of attack much like a wing under these conditions, and, as Glauert was to show, the aerodynamics of the rotor are very much like a fixed-wing of circular planform under these conditions.

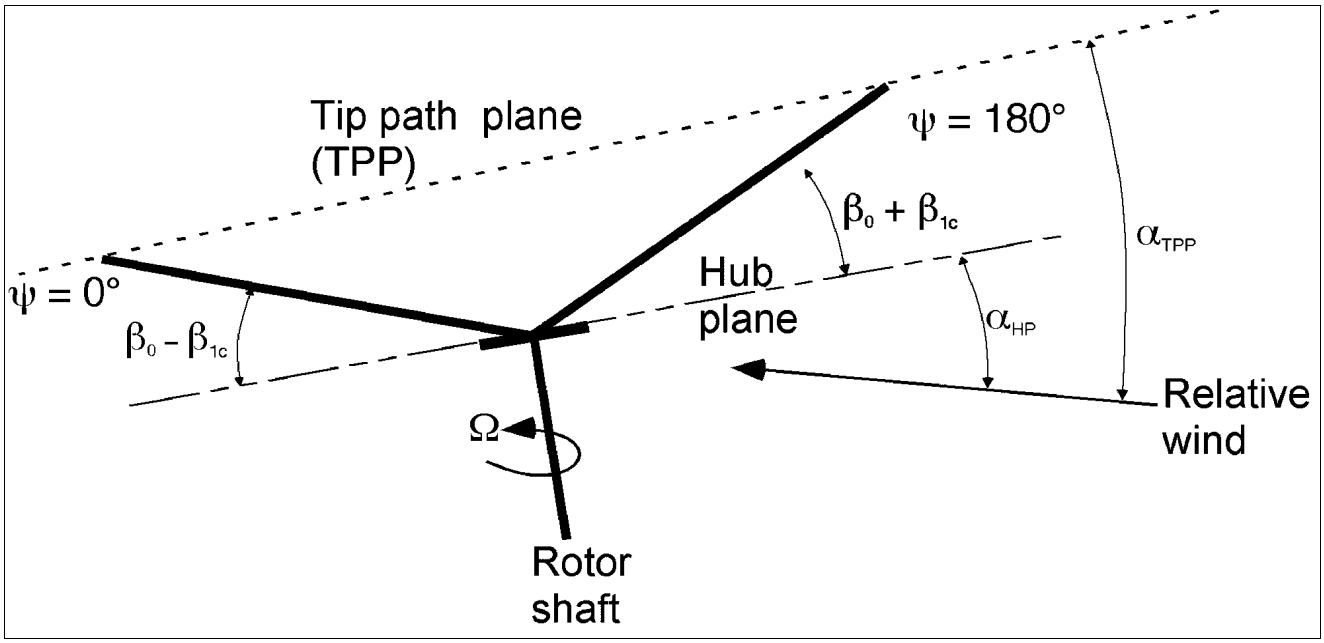

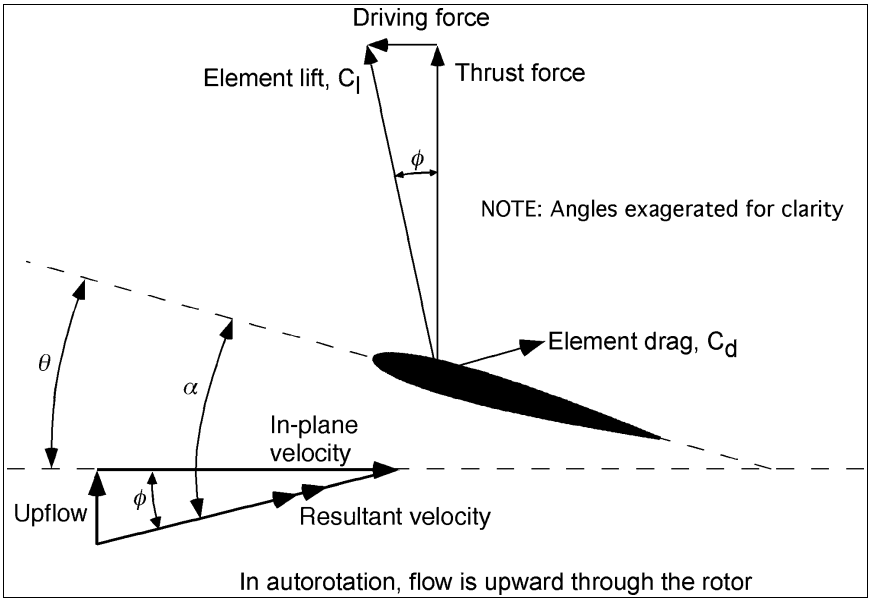

There are a number of combinations of rotor operating conditions where the net torque on the rotor shaft could be zero. Consider the flow environment encountered at a blade element on the rotor during auto rotation, as shown in the figure on the left. For auto rotational equilibrium at that section, the inflow angle φ must be such that there is no net in-plane force and, therefore, no contribution to rotor torque, that is, for force equilibrium

$$dQ = (D - \varphi L)\, ydy = 0$$

$$ydy \neq 0$$

$$(D - \varphi L) = 0 = Cd - \varphi Cl$$

However, this is an equilibrium condition that cannot exist over all parts of the blade, and only one radial station on the blade can actually be in auto rotational equilibrium. In general, some portions on the rotor will absorb power from the relative air stream, and some portions will consume power, such that the net torque at the rotor shaft is zero, that is, dQ = 0. With the assumption of uniform inflow over the disk, the induced angle of attack at a blade element is given by:

$$\varphi = \frac{Upflow\, velocity}{Inplane\, velocity} = \arctan\left(\frac{|Vc + vi|}{\Omega}\right)$$

It follows that for auto rotational equilibrium the induced angles of attack over the inboard stations of the blade are relatively high, and near the tip the values of φ are relatively low.

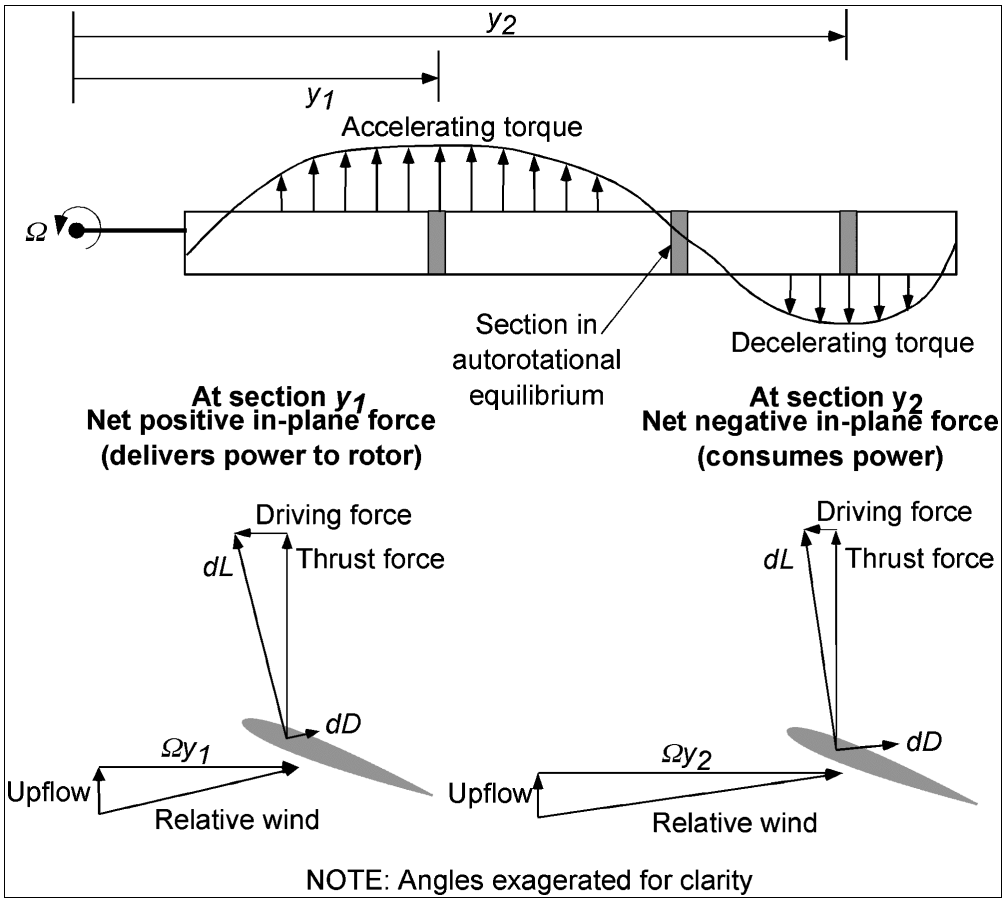

One finds that at the inboard part of the blade the net angle of attack results in a forward inclination of the sectional lift vector, providing a propulsive component greater than the profile drag and creating an accelerating torque, a fact known by De la Cierva. This blade element can be said to absorb energy from the relative air stream. Toward the tip of the blade where φ is lower, these sections of the blades consume energy because the propulsive component as a result of the forward inclination of the lift vector is insufficient to overcome the profile drag there, that is, a decelerating torque is produced.
As De la Cierva understood, in the fully established auto rotational state the rotor rpm will adjust itself until a zero torque equilibrium is obtained. This is a stable equilibrium point because it can be deduced from last figure above that if Ω increases φ will decrease and the region of accelerating torque will decrease inboard, and this tends to decrease rotor rpm again. Conversely, if the rotor rpm decreases then φ will increase, and the region of accelerating torque will grow outward. **Therefore, when fully established in the auto rotative state the rotor naturally seeks to find its own equilibrium rpm to any changing flight conditions.** This is an inherent characteristic of the rotor that gives the autogiro very safe flight characteristics theoretically. However, in the auto rotational state the blade pitch must always be at a low value, and the disk angle of attack must be positive to ensure that the inboard blade sections never reach high enough angles of attack to stall. Stall can occur if the rotor rpm goes below an acceptable threshold, such as when the disk angle of attack becomes negative, or a negative load

factor is produced. These are flight conditions to be avoided. If stall does occur, then the outward propagation of

stall from the blade root region will tend to quickly further decrease rotor rpm because of the associated high profile drag. The phenomenon of auto rotation is often explained using an auto rotational diagram.

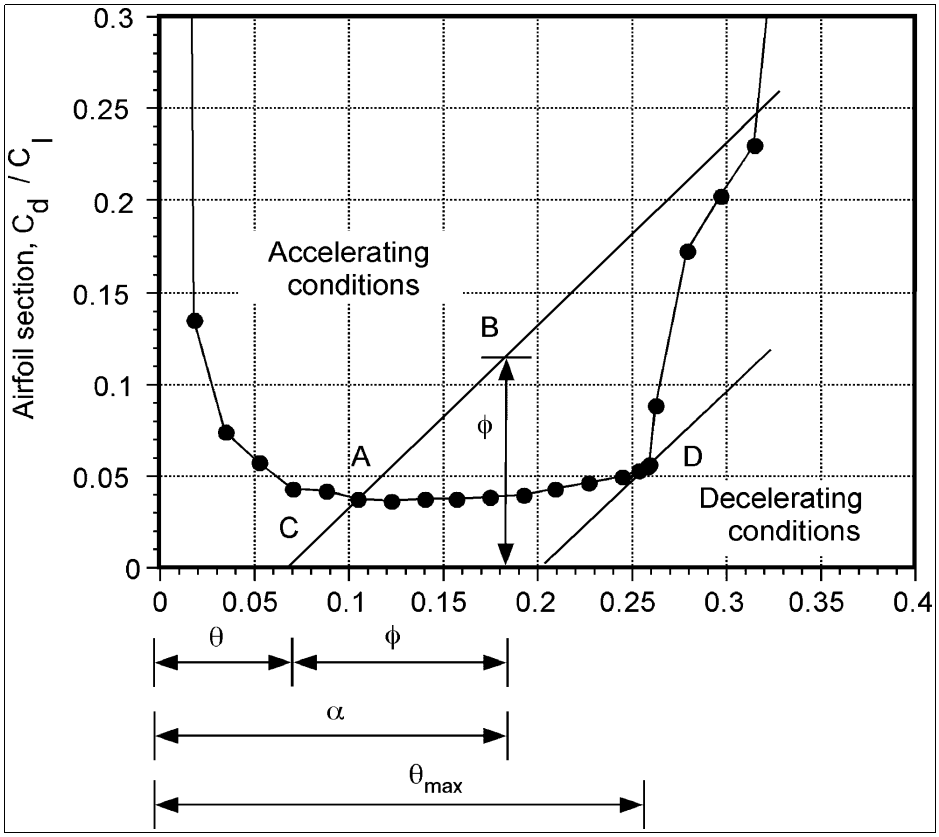

This is shown in the figure above, where the blade section Cd /Cl is plotted vs angle of attack at the blade section. For a single section in equilibrium,

$$Cd - \varphi Cl = 0 \qquad \frac{Cd}{Cl} = \varphi = \alpha - \theta$$

For a given value of blade pitch angle θ and inflow angle φ, the preceding equation represents a series of points that form a straight line, which is plotted on the diagram above. The intersection of this line with the measured Cd/Cl data for the airfoil sections comprising the rotor blades at point A corresponds to the equilibrium condition where φ = Cd /Cl . Above this point, say at point B, φ > Cd /Cl , so this represents an accelerating torque condition. Point C is where φ < Cd /Cl , and so this represents a decelerating torque condition. Note that above a certain pitch angle, say θmax, equilibrium conditions are not possible, so for point D stall will occur causing the rotor rpm to quickly reduces, an issue alluded to earlier.

When a rotor operates in forward flight with the rotor passing edgewise through the air, the rotor blades encounter an asymmetric velocity field (see figures below).

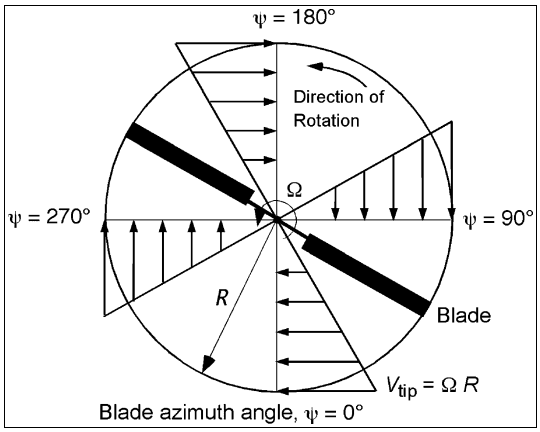

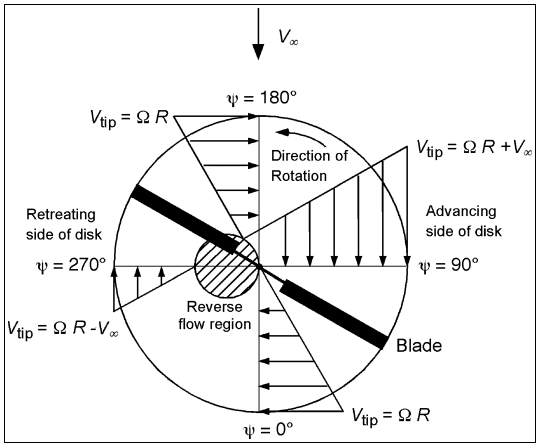

The blade position can be defined in terms of an azimuth angle ψ, which is defined as zero when the blade is pointing downstream. The local dynamic pressure and the blade airloads now vary in magnitude with respect to blade azimuth, and they become periodic (primarily) at the rotational speed of the rotor, that is, once per revolution or 1/rev. It will be apparent that the aerodynamic forces must reach a maximum on the blade that advances into the relative wind (i.e., at ψ = 90 deg), and will be minimum on the blade that retreats away from the relative wind (i.e., at ψ = 270 deg). For blades that are rigidly attached to the shaft, the net effect of these asymmetric aerodynamic forces is an upsetting moment on the rotor. This was de la Cierva's first dilemma in developing the autogiro.

It will be evident that the distribution of lift and induced inflow through the rotor will affect the inflow angles φ and angles of attack at blade sections and, therefore, the detailed distribution of aerodynamic lift and drag forces over the rotor. This subsequently affects the blade-flapping response, and therefore the aerodynamic loads. This interrelated behavior is a complication with a rotating wing that makes its thorough analysis relatively difficult, a fact well appreciated by De la Cierva and is still the subject of much research today.

Notice also from figure above right that at higher forward speeds (advance ratios) a region of reverse flow (and stall) will form at the root of the retreating blade, increasing rotor profile drag and reducing aircraft performance.

De la Cierva's first Autogiro, the C-1, was built in 1920 and had a coaxial rotor design. He was to build two more machines, both with single rotors, before he achieved final success with the C-4 in January 1923. The problem of asymmetric lift between the advancing and retreating blades was well known to De la Cierva. His first idea of using a counter-rotating coaxial design was that the lower rotor would counteract the asymmetry of lift produced on the upper rotor, thereby balancing out any moments on the aircraft. However, when flight tests began it was found that the aerodynamic interference between the rotors resulted in different auto rotational rotor speeds. This spoiled the required aerodynamic moment balance, and the C-1 capsized before becoming airborne. De la Cierva considered the possibility of mechanically coupling the rotors to circumvent the problem, but this was quickly rejected because of the obvious mechanical complexity and significant weight penalty. Despite its failure to fly,

however, the C-1 proved that the rotors would freely auto rotate when the machine was taxied with sufficient forward speed. The next Cierva design was the compensating rotor, which was tested in three-bladed form on the C-3 in 1921 and in five-bladed form on the C-2 in 1922. (The C-2 actually followed the C-3.) This idea used blade twisting in an attempt to compensate for the undesirable characteristic of asymmetric lift, that is, by using nose-down twist on the advancing blade and nose-up twist on the retreating blade. Photographs of these two machines show a series of cables attached to the trailing edges of the blades, with the idea that the blade twist could be changed in a cyclic sense as the blades rotated about the shaft. However, although the basic principle was correct the concept proved impractical, and both the C-2 and C-3 were only to achieve short hops off of the ground. Perhaps the use of cyclic blade feathering (as opposed to blade twisting) might have been more successful, but it was not to be until 1931 that E. Burke Wilford in the United States demonstrated this concept on an auto giro. NACA was also to study this type of rotor in wind tunnel.

Based on his many experiments with small models, De la Cierva noticed that the flexibility of the rattan spars on his models provided different aerodynamic effects compared to the relatively rigid blade structure used on his full-scale machines. This was the key De la Cierva needed and his “secret of success.” His fourth machine (the C-4), therefore, incorporated blades with mechanical hinges (horizontal pins) at the root, which allowed the blades to freely flap up and down in response to the changing asymmetric aerodynamic lift forces during each rotor revolution (see schematic in the figure below).

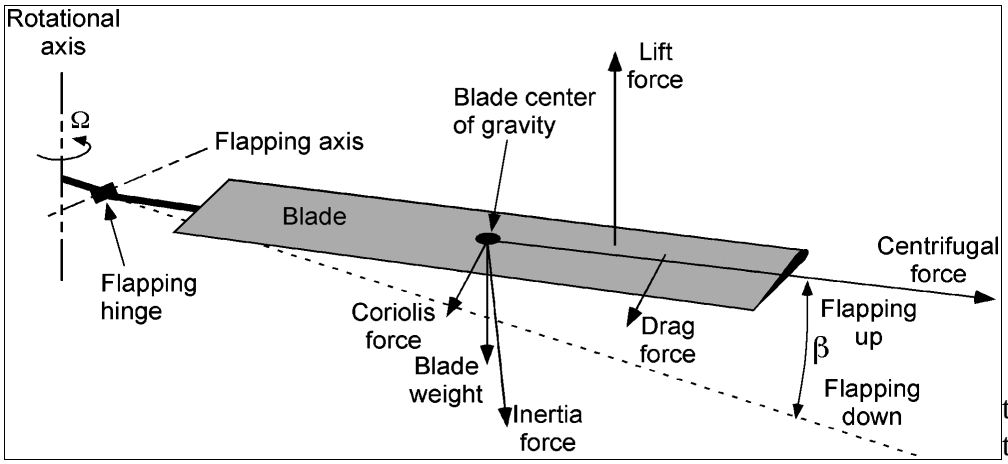

Also acting on the blades are centrifugal and gravitational forces, and as a result of free flapping there are inertia and Coriolis forces to contend with, all of which act through the center of gravity of the blade. The blades on the C-4 were restrained by cables attached to the shaft to limit both lower and upper flapping angles, and also so the blades would not droop to the ground when the rotor was stopped.

The principle of flapping blades had actually first been suggested for the application to propellers, apparently by Charles Renard, but the idea of hinged blades was formally patented by Louis Breguet in 1908 and then by Max Bartha and Josef Madzer in 1913. Juan De la Cierva, however, must be credited with the first successful practical application of the flapping hinge to a rotor. From his various writings it does not seem that Cierva was aware of any of the earlier ideas of flapping blades. De la Cierva noticed that the incorporation of the flapping hinge eliminated any adverse gyroscopic effects and also allowed the lift forces on the two sides of the rotor to become more equalized in forward flight.

However, de la Cierva's initial avoidance of using a lead-lag hinge to alleviate the in-plane blade Coriolis forces (resulting from the flapping motion) and in-plane blade motion was an oversight that he was ultimately to come to terms with (see later).
In de la Cierva's C-4 Autogiro of 1923, a single rotor with four independent, freely flapping blades was mounted on a long shaft above an Avro airplane fuselage. The blades were of high aspect ratio, similar to those of modern helicopter blades, and used a relatively efficient Gottingen 429 airfoil shape. A propeller, powered by a Le Rhone gasoline engine, provided propulsion. The first model of the C-4 used a lateral tilting of the entire rotor disk to provide roll control and without the use of any auxiliary "fixed" wings, which were later to be characteristic of most of his Autogiros. However, taxiing tests showed that the control forces involved in tilting the rotor were too high for the pilot, and the control response also proved very ineffective. The machine was subsequently fitted with a non- tilting rotor and a set of ailerons mounted on a stub spar projecting from the sides of the fuselage. Pitch and directional (yaw) control on the C-4 was then achieved by conventional airplane surfaces, with an elevator and a rudder used at the tail.

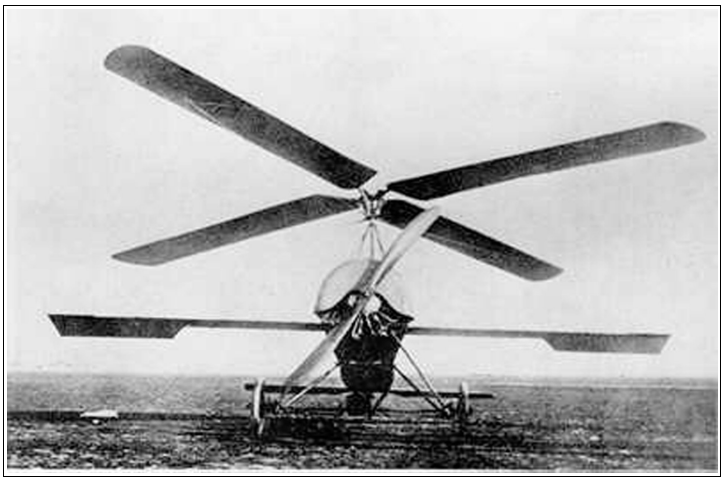

The C-4 Autogiro first flew successfully on 9 January, 1923 (see figure below-left) and made its first official flight demonstrations at the Getafe Aerodrome in Madrid on 21 January, 1923. On 31 January, 1923 at the Quatro Vientos Aerodrome, the C-4 was flown around a 4-km
closed circuit, and this was to be the first time any flying machine other than a conventional airplane had accomplished this feat. It took De la Cierva just over a year between conceiving the idea of the flapping hinge and using it to successfully fly the first autogiro.

This part should be read after the chapter n°5, but it would be better placed in the general theory.

Two main conditions have to be fulfilled during a steady axial flight in auto rotation; rotor thrust has to be in balance with the weight of the vehicle and the overall torque generated by the flow through the rotor disc has to be zero .

$$T = Mg$$
$$Q = 0$$

The thrust equation can be consequently used for calculation of rotor speed. The inflow ratio can be computed once rotor speed is calculated with the aid of the zero aerodynamic torque condition. An analytical or empirical relation between the vertical component of inflow velocity Up and the speed of descent Vd can be used to estimate the rate of descent of a rotor in auto rotation. This is equivalent to the relationship of thrust coefficient based on resultant air velocity F and thrust coefficient based on descending velocity f .

$$F = \frac{T}{2\pi R^2 \rho Up^2} \qquad f = \frac{T}{2\pi R^2 \rho Vd^2} \qquad \frac{f}{F} = \left(\frac{Up}{Vd}\right)^2$$

Several experimental measurements were carried out to determine the relationship between $\frac{1}{F}$ and $\frac{1}{f}$. Reproduced from Trchalik

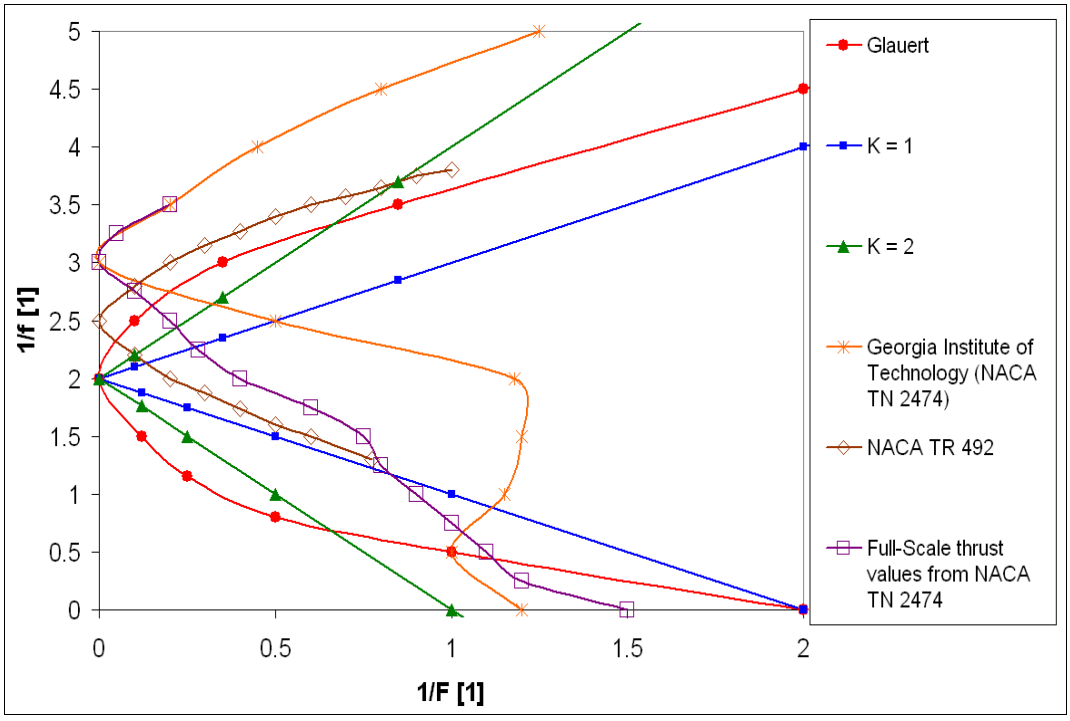

Nikolsky and Seckel also gives an analytical approximation of relationship between

$\frac{1}{F}$ and $\frac{1}{f}$.

$$\frac{1}{f}=2\pm K\frac{1}{F};\quad |K|\in\langle 1,2\rangle$$

A positive value of K corresponds to the windmill brake-state (i.e. the upper branch of F-curve) and a negative K indicates that the rotor is in the vortex ring state (VRS; the lower branch of F-curve) .

Rotor inflow ratio can be calculated (for the blade element, NB = number of blades) as :

$$\lambda=\frac{\frac{-cL\alpha E\theta}{4}+\sqrt{(\frac{cL\alpha E\theta}{4})^2+(\frac{cL\alpha E}{3}-\frac{cDE}{2})(\frac{cDE}{4}+\frac{2Q}{NB\rho\Omega^2R^4cE})}}{\frac{2cL\alpha E}{3}-cDE}$$

Once the inflow ratio is calculated, the inflow speed can be obtained with the help of the following equations :

$$\lambda D=\sqrt{\frac{T}{f\,2\pi\rho\Omega^2R^4}}$$

$$vi=\Omega R(\lambda D-\lambda)$$

Note.

The modified version by a classic Glauert's $vi(x,psi)=\frac{T}{2\pi R^2\rho Vh}*(1+1.2*r(x)*\cos(psi))$ *model works quite well in my software.*

4. Typical parameters

It's clear that the auto rotative performance of an autogyro depends on several interrelated factors. These include the rotor disk loading (which affects the descent rate), the stored kinetic energy in the rotor system (which influences the probability of success of entry and completion of the maneuver), as well as "difficulty rating" flight assessment by pilots.
To help select the rotor diameter during predesign studies, an "autorotative index" is often used.
Although various types of typical numbers have been used, the A.I. is basically a stored kinetic energy factor. One form of the index can be defined in terms of the ratio of kinetic energy of the main rotor to the gross weight of the craft. That is (Sirkorsky),

$$A.I. = \frac{Ir\Omega^2}{2W\,D.L.}$$

where D.L. Is the disk loading, and Ir is the polar inertia momentum of the rotating disk In a general way, the lower A.I. is, the safest flight we obtain.
Example:

D.L.= 1,5 kg/m^2 (15 g/dm^2)
Ω = 21 rad/s (200 rev/min)
Ir = 0,125 kgm^2
W = 15 N

A.I. = 12.25 (good result)

Now we introduce a useful way to determine the power needed by the autogyro in forward flight. We say the rotor total lift coefficient CL:

$$CL = \frac{W}{\frac{1}{2}\pi R^2 \rho V^2}$$

The rotor speed can now be estimated by assuming a control axis tilt less than 10° such that:

$$\Omega = \frac{V}{\mu R}$$

The rotor-drag lift ratio is defined as:

$$\left(\frac{D}{L}\right)r = \left(\frac{D}{L}\right)i + \left(\frac{D}{L}\right)0$$

$$\left(\frac{D}{L}\right)i = \frac{kCT}{2\mu^2};\ 1.1 \leqslant k \leqslant 1.2 \qquad \left(\frac{D}{L}\right)0 = \frac{\sigma Cd}{8}\frac{1+4.6\mu^2}{\mu CT}$$

$$(\frac{D}{L})i \simeq \frac{CL}{4}$$

We've got $(\frac{D}{L})0$ from the chart below:

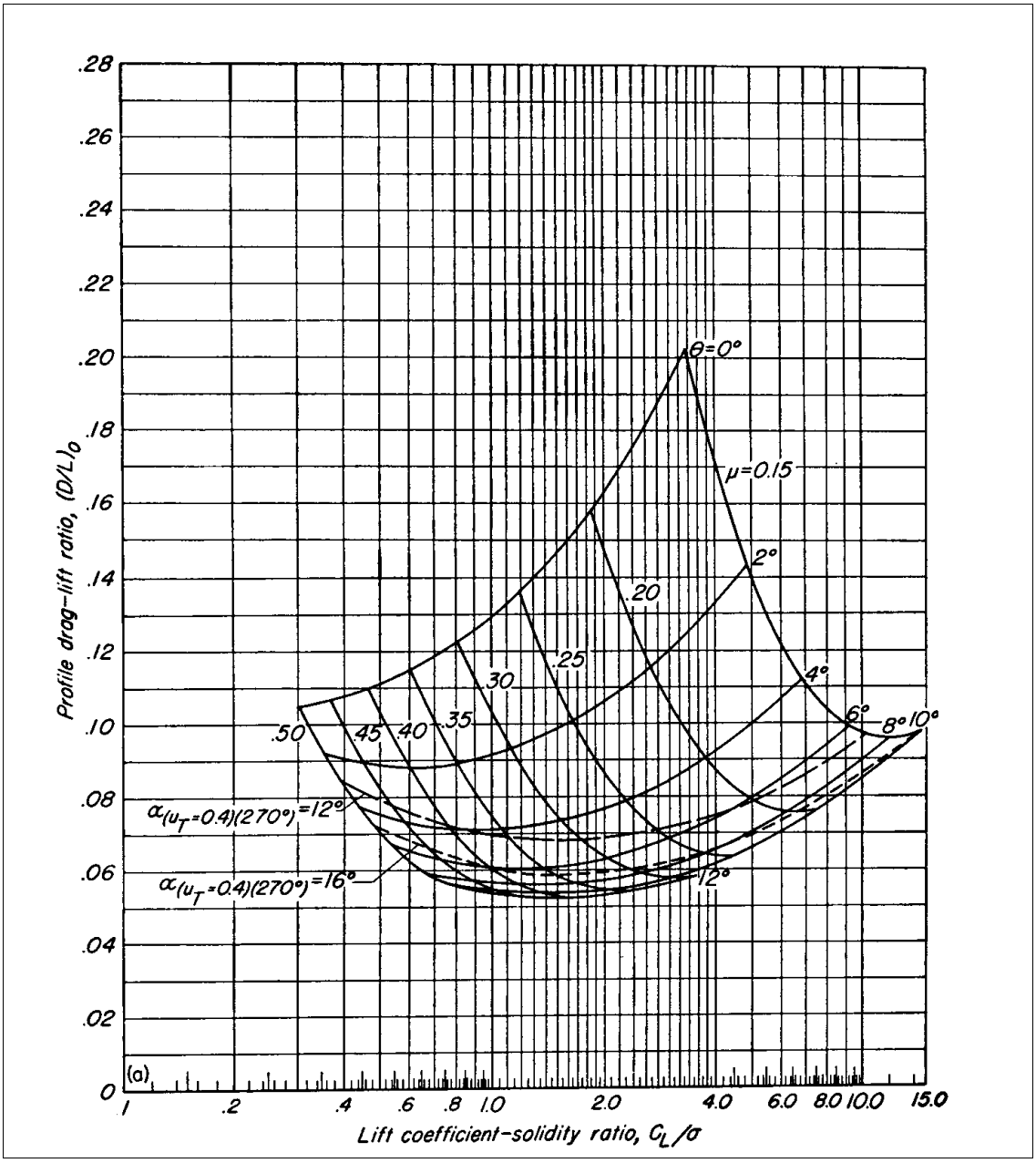

The total drag is calculated as:

$$D=(\frac{D}{L})r\,W$$

The parasite drag Dp is calculated from the coefficient Cpd and the forward speed V. So the total drag Dt becomes:

$$Dt=Dr+Dp=(\frac{D}{L})r\,W+Cpd\,(\frac{1}{2})\rho V^2$$

We can give an estimation of Dp such as Dr/4.

The power required can now be calculated as: $Preq=DV$

The calculation of the propeller thrust comes from the standard Hamilton method with some simplifications.
For a given density ratio $\frac{\rho}{\rho 0}$, the propeller coefficient Cp' is calculated as:

$$Cp'=\frac{3.325\,10^{10}\,HP}{N^3(\frac{d}{0.304})^5\frac{\rho}{\rho 0}}$$

Where HP is the engine power, and $\frac{\rho}{\rho 0}=1$ at sea level.

From the figure below we evaluate a measure (at a tip speed of ≈270 m/s-900 ft/s) of the static thrust coefficient:

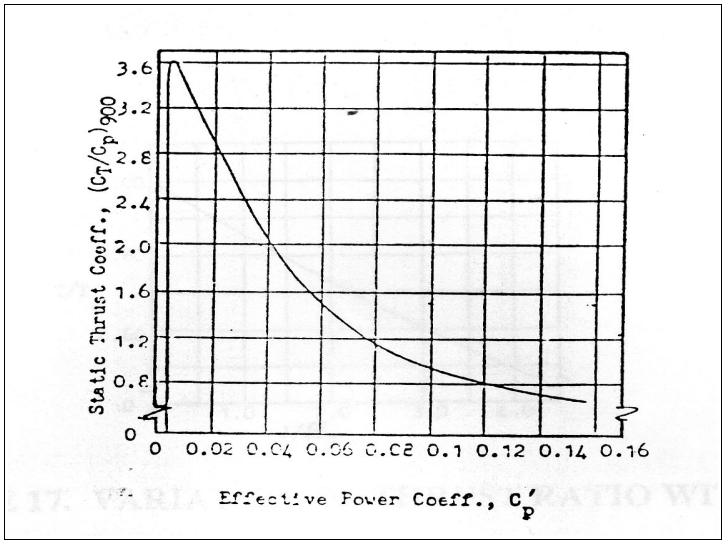

$$Ts=(\frac{Ct}{Cp})\frac{HP\,0.93.3\,10^4}{N\,(\frac{d}{0.3048})}$$

The flight thrust as a function of the airspeed is found by the following relation:

$$\frac{J}{\sqrt{Cp}}=2.84\,V\sqrt{\frac{N\,(\frac{d}{0.3048})^3\,\frac{\rho}{\rho 0}}{HP\,10^7}}$$

We find the flight thrust to static trust ratio from the following chart:

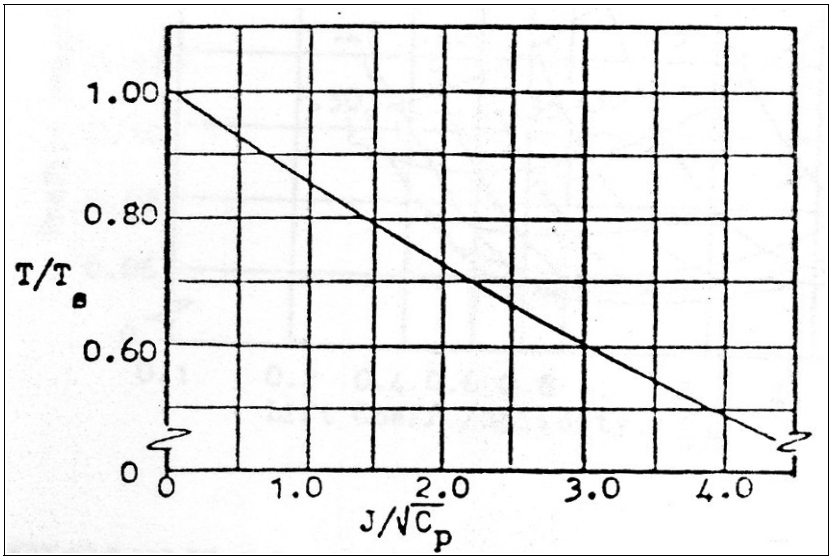

Finally the propeller thrust available is:

$$Pav=T\,V$$

For HP=0.5 Hp, N=12000 rev/min, d=0.2 m (prop diam), W=15 N, B=4, c=0.05, R=0.5, θ=4°, μ=0.25.

V (km/h)	**V (m/s)**	$\frac{J}{\sqrt{Cp}}$	$\frac{T}{Ts}$	T	Pav	Cl	$\frac{Cl}{\sigma}$	$(\frac{D}{L})0$	$(\frac{D}{L})i$	$(\frac{D}{L})r$	Dr	Dp	D	$Preq$
60	16.7	1.23	0.85	1.8 N	31 W	0.09	2.83	0.07	0.02	0.09	1.35 N	0.3 N	1.65 N	27.5W

5. Mathematical Blade Models

Some parts of this chapter are from University of Glasgow - Trchalik -UK.

The mathematical model of the autogyro blades are focused on the elastic behavior of the blades subjected to the lifting forces and inertial forces (centrifugal and Coriolis). The behavior of the blades during flight is well visible in the two pictures here below (Glasgow University - Trchalik).

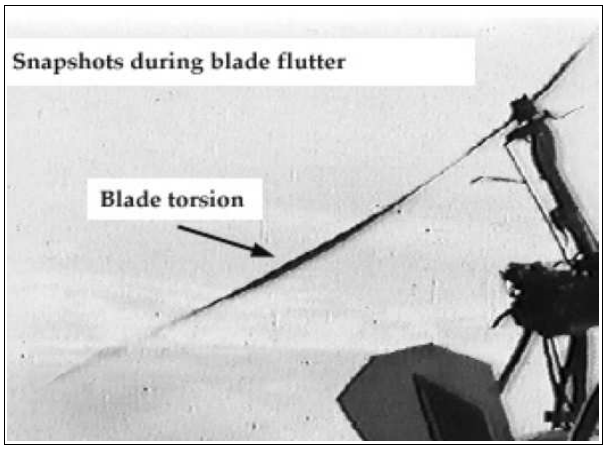

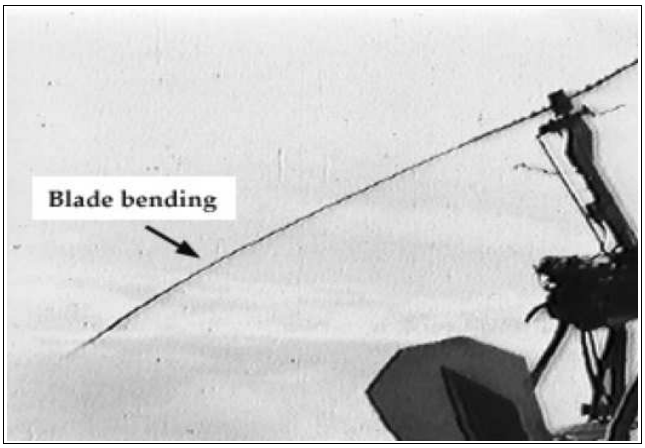

Cierva's problems with excessive torsion of rotor blades forced designers of the first modern helicopters to use symmetrical (uncambered) airfoils. Better understanding of helicopter rotor dynamics allowed use of cambered, high-performance airfoils in later generations of helicopter designs .
Excessive torsion of rotor blades was avoided with the aid of stiffer rotor blades and amended arrangement of blade hinges. A pitch-flap flutter is avoided by placing a mass balance at the blade tip.
Since the speed of gyroplane rotors is not mechanically restricted, it depends on aerodynamic loading of the rotor. Reflex camber airfoils are now used in the design of modern gyroplane rotors as they generate positive (nose-up) pitching moment that reduces rotor torque and hence decreases aerodynamic loading. This allows establishing of a balance between rotor speed and span-wise distribution of blade incidence.

In general, analytical methods required for modelling of the aerodynamics of auto rotating rotors are similar to those developed for helicopter rotors in powered flight.
However, several modifications have to be made in the blade element aerodynamic model of a helicopter rotor in order to reflect different character of the aerodynamics of a rotor in auto rotation.

As with helicopter rotor blades, rotor blades in autorotation are subjected to high vibratory loading for most of the time. The blades are also highly flexible. Structural loading can reach even higher values than in the case of helicopters since the blades can experience significant fluctuation of centrifugal stiffening due to decrease of rotor speed. Additional components of aerodynamic angle of attack that are caused by blade oscillatory motion have to be considered. This can be done with the aid of the

quasi-steady or the unsteady (Theodorsen's) aerodynamic theory. The airflow around a rotor blade can be considered quasi-steady if the reduced frequency of blade motion is lower than 0.05.
Reduced frequency is defined as follows:

$$k=\frac{\Omega c}{2V}$$

Classical formulations of quasi-steady lift and moment coefficient as given by Leishman are :

$$Cl=2\pi\left[\alpha+\frac{\dot{h}}{V}+b\left(\frac{1}{2}-a\right)\frac{\dot{\alpha}}{V}\right]$$

$$C(M,4)=\frac{-\pi}{4}\frac{\dot{\alpha}\,b}{V}$$

α steady angle of attack [rad]
$\dot{\alpha}$ rate of change of angle of attack [rad/s]
a = offset of the pitch axis from half-chord
b = half-chord, b = c/2

Vertical displacement of local blade sections wp is more consistent with the rotor coordinate system and rotor blade dynamics that were used in this work and in the model.

$$\dot{w}=-\dot{h}=\dot{w}\cos(\theta)$$

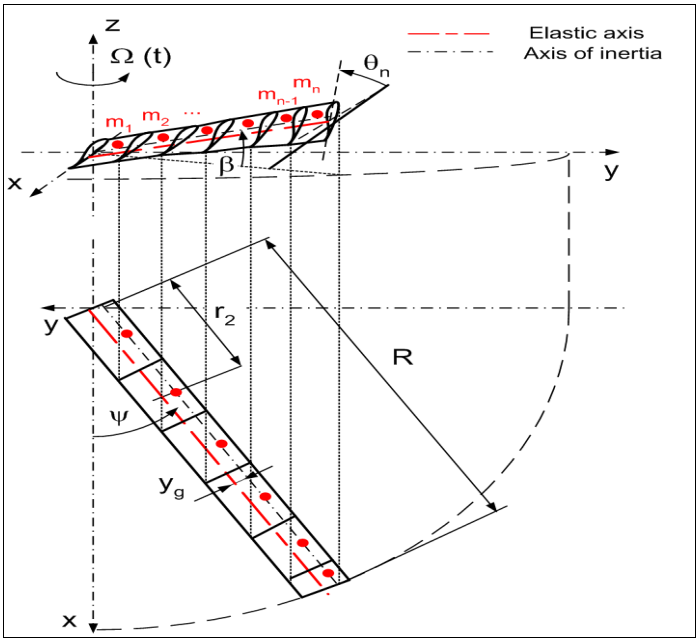

Hence the classical formulations of quasi-steady lift and moment coefficients generated by a blade section has to be rewritten in order to be consistent with the coordinate system orientation of the model

$$Cl = 2\pi\left[\alpha + \frac{1}{\Omega r}\left(-\dot{w}\, p + \left(\frac{3c}{4} - yEA\right)\dot{\theta}\right)\right] \quad cl\alpha = 2\pi$$

$$C(M,4) = \frac{-\pi}{8}\frac{\dot{\theta}\, c}{\Omega r}$$

Hence the equation can be written in a simpler form :

$$CL = CL\alpha\left(\alpha + \alpha q\right)$$

Where:

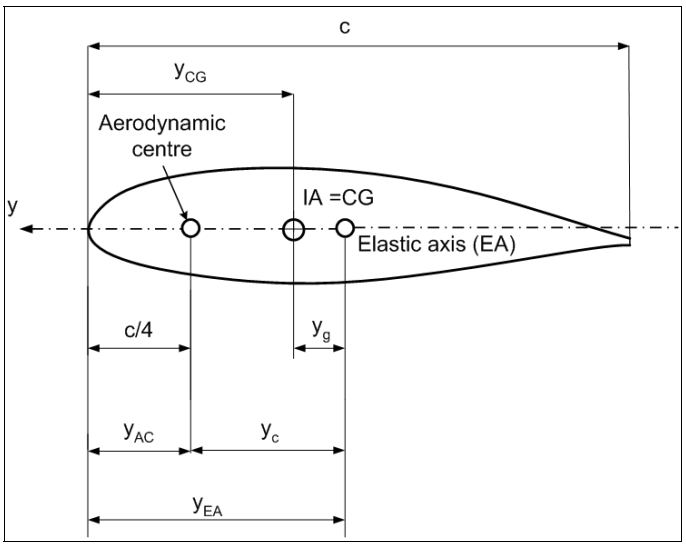

αq is the quasi-steady angle of attack [rad] and yEA is the local chord-wise position of elastic axis [m] . wp = wcosθ.

Local values of vertical and horizontal components of the inflow velocity (U) have to be calculated in order to determine aerodynamic angle of attack of any blade section. The inflow velocity can be projected into three components (Up, Ut, Ur). Vertical component of inflow velocity Up describes air speed of the flow in direction perpendicular to the rotor disc, Ut is parallel with the rotor disc plane and perpendicular to the longitudinal axis of the blade and Ur is parallel with both rotor disc plane and the blade axis.

.

Aerodynamic angle of attack of a blade section in auto rotation is

$$\alpha = \theta + \varphi = \theta + \arctan\left(\frac{Up}{Ut}\right)$$

In forward flight, however, the value of Ut can be negative in the reverse flow region of the rotor disc. In order to capture the reverse flow, the definition of inflow angle has to be modified. In a simpler way, the value of the inflow velocity can be calculated as :

$$\varphi RF =$$

$$\varphi \ if \ \ Ut \geq 0$$

$$\varphi + \pi \ if \ \ U < 0$$

The inflow velocity is a function of angle of attack of the rotor disc that is given by a sum of incidence angle of the rotor disc i (i.e. angle between the rotor disc plane and the horizontal plane) and pitch angle of the vehicle.

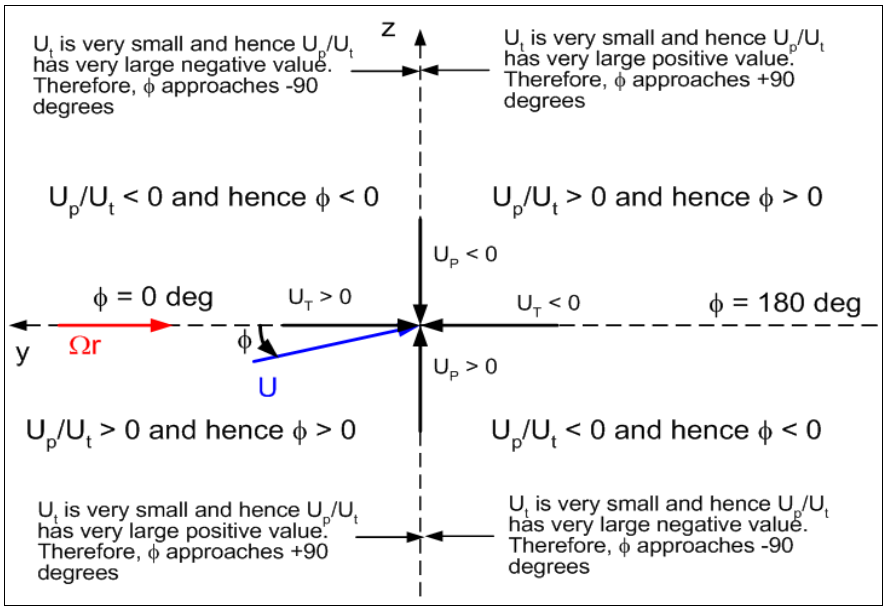

Referring to figure below analytical expressions of individual components of the inflow velocity of a gyroplane rotor can be formulated, including the effect of longitudinal and lateral rotor disc tilt (i and iL)

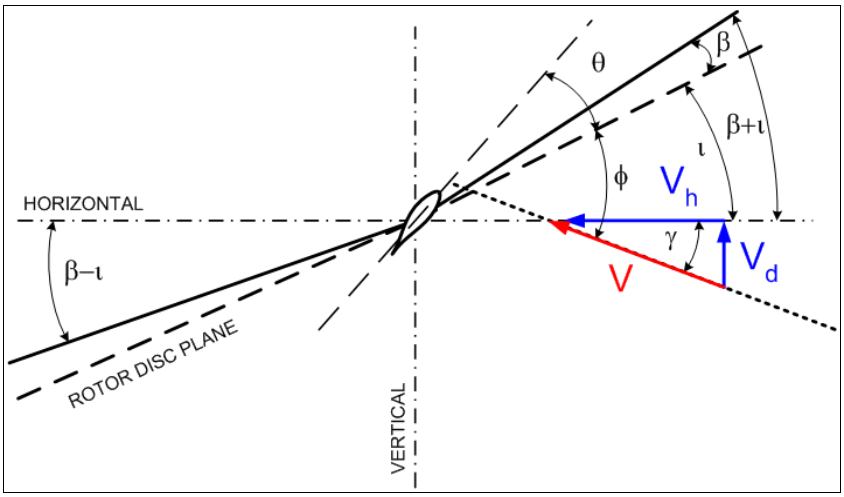

$$\alpha d = i + \gamma$$

$$\gamma = \arctan\left(\frac{Vd}{Vh}\right)$$

Note that if the rotor disc incidence angle is zero, the flapping angle is assumed to be very small and the three expressions of Up, Ut and Ur are :

$$Up = \Omega R[\lambda - \mu\beta cos\psi - \frac{x}{\Omega}\dot{\beta} + (\frac{3}{4c} - yEA)\frac{\dot{\theta}}{\Omega}]$$

$$Ut = \Omega R(x + \mu \sin\psi)$$

$$Ur = \Omega R(\mu \cos\psi - \lambda\beta)$$

where:

$$\beta \quad Rotor\,blade\,flapping\,angle[rad]$$

$$\lambda \quad Inflow\,ratio, \lambda = \frac{Vd - vi}{\Omega R}$$

$$\mu \quad Advance\,ratio, \mu = \frac{VH}{\Omega R}$$

$$\psi \quad Azimuth[rad]$$

$$x \quad Dimensionless\,span - wise\,coordinate \quad x = \frac{r}{R}\; yEA \quad is\,the\,local\,chord - wise\,position\,of\,elastic\,axis[m]$$

The equations above represent the classical form of rotor inflow equations that have been broadly used for aerodynamic analysis of helicopter rotors in auto rotation .

Once aerodynamic angles of attack of each blade element are calculated, they can be used for estimation of the aerodynamic loading of the rotor blades. In order to achieve this, relationships between the aerodynamic angle of attack of blade sections and lift, drag and pitching moment coefficients have to defined.

This can be done in several possible ways, depending on desired accuracy of estimation of blade aerodynamic loading.
It is more convenient to express the aerodynamic characteristics of the blade airfoil as polynomial functions of angle of attack and Mach number. At least two different polynomials have to be used; the first polynomial is used for the area of angles of attack between α = -25deg and α = 25deg. The outboard sections of rotor blades (which generate a major part of the rotor forcing) operate in this range of angles of attack most of the time, and hence an approximation of this part of the lift and drag curves should be more accurate. The trend of both lift and drag curves outside this region can be approximated with the aid of simple trigonometric functions.
It was shown by Prouty that it is possible to obtain the full-range angle of attack aerodynamic data of an airfoil with the aid of numerical approximation. Prouty uses NACA 0012 airfoil in his book (Helicopter Performance, Stability and Control) as an example. This type of airfoil was widely used in the field of rotorcraft aerodynamics and an ample amount of experimental data are available for this airfoil. Prouty's amended compressibility correction :

$$cL\alpha = \frac{C1}{\sqrt{1 - M^2}} + C2M$$

For NACA 0012, C1 = 0.1 deg^{-1} and C2 = −0.01 deg^{-1} . Prouty assumes that for a low speed airflow, the slope of linear part of NACA 0012 lift curve is cLα = 5.73 rad^{-1}.

$$\alpha L = C3 + C4\,M$$

For NACA 0012, C3 = 15 deg and C4 = −16 deg.
Hence, for values of angle of attack lower than αL (linear part of lift-curve) and above αL , values of lift coefficient of the airfoil can be estimated as follows :

$$cL = cL\alpha\,\alpha$$
$$cL = cL\alpha\,\alpha - C5\,(\alpha - \alpha L)^{C6}$$

$$C5 = -0.4375\mathrm{M}^5 + 3.492\mathrm{M}^4 - 5.3304\mathrm{M}^3 + 3.4269\mathrm{M}^2 - 1.0074\mathrm{M} + 0.12334$$
$$C6 = 67.0833\mathrm{M}^5 - 152.8561\mathrm{M}^4 + 143.6822\mathrm{M}^3 - 72.3092\mathrm{M}^2 + 18.6842\mathrm{M} + 0.2004$$

Prouty's method of polynomial fit of airfoil drag curve was enhanced in order to capture the effect of reverse flow.

$$cD1 = 1.03 - 1.02\cos 2\alpha$$
$$cD2 = 5.0885 - 1.7192\cdot 10^{3}\alpha + 2.4138\cdot 10^{1}\alpha^{2} -$$
$$+ 1.8027\cdot 10^{-}1\,\alpha^{3} + 7.5522\cdot 10^{-}4\,\alpha^{4} -$$
$$1.6828\cdot 10^{-}6\,\alpha^{5} + 1.5582\cdot 10^{-}9\,\alpha^{6}$$

In the reverse flow region:

$$cD, revf =$$
$$cD1\ if\ cD2 > cD1$$
$$cD2\ if\ cD1 > cD2$$

For angles of attack below the stall, moment curve of NACA 0012 can be expressed in the following way (α rad) :

$$cM, \alpha < 20\deg(\alpha, M) = M0 + M1\,\alpha + M2\,\alpha^{2} + M3\,\alpha^{3} + M4\,\alpha^{4} + M5\,\alpha^{5}$$

We can only estimate the cM, because the Prouty model reported on Trchalik's thesis is for real applications, not for models.

M	**0th order**	**1th order [rad−1]**	**2th order [rad−2]**
0.3	$-5.319\cdot 10^{-5}$	$-3.425\cdot 10^{-1}$	$1.5213\cdot 10$
M	**3th order [rad−3]**	**4th order [rad−4]**	**5th order [rad−5]**
0.3	$-1.875\cdot 10^{2}$	$9.468\cdot 10^{2}$	$-1.666\cdot 10^{3}$

$$cM, \alpha > 20\deg =$$
$$0.08 + 0.4\sin(0.4\alpha^{1.8})\ \ if\ \ 20\deg \le \alpha \le 166\deg$$
$$0.4\sin(0.898\alpha^{2.5})\ \ if\ \ 166\deg < \alpha \le 180\deg$$

Once aerodynamic coefficients at all span-wise stations are obtained, the aerodynamic forces and moments generated by the blade elements can be calculated.
Lift and drag force and pitching moment at quarter-chord generated by an arbitrary element of the rotor blade of width dr are shown in their standard formulations :

$$dL = \frac{1}{2} cL\, \rho c U^2 dr$$

$$dD = \frac{1}{2} cD\, \rho c U^2 dr$$

$$dM\left(\frac{c}{4}\right) = \frac{1}{2} cM\left(\frac{c}{4}\right) \rho c^2 U^2 dr$$

Lifting force is perpendicular to the direction of inflow velocity and drag force vector is perpendicular to the vector of lift force. Local values of inflow angle and angle of attack have to be used to obtain forcing moments of the blade. Elementary rotor thrust and in-plane force (frequently called H-force) are defined by the following equations :

$$dT = dL \cos\varphi + dD \sin\varphi$$
$$dH = dL \sin\varphi - dD \cos\varphi$$

Numerical integration has to be used in an aerodynamic model based on the blade element method. This approach is both simple and accurate, especially if a high number of span-wise elements is used. Hence numerical integration is especially useful in computer-aided modelling of rotor aerodynamics. Arbitrary span-wise distributions of blade properties and flow conditions can easily be captured and the full form of blade aerodynamic equations can also be used.
Using numerical integration, aerodynamic forcing moments can be expressed in a form that can be used for a blade element model of an auto rotating rotor (i=1, N elem) :

$$M\psi, A = \sum i\left[\frac{1}{2} \rho ci\, \Omega^2 ri^3 \left[cL\alpha, i \sin\varphi i\, (\alpha i + \alpha q, i) - cD, i \cos\varphi i\right] \Delta ri\right]$$

$$M\beta, A = \sum i\left[\frac{1}{2} \rho ci\, \Omega^2 ri^3 \left[cL\alpha, i \cos\varphi i\, (\alpha i + \alpha q, i) + cD, i \sin\varphi i\right] \Delta ri\right]$$

$$M\theta, A = \sum i\left[\frac{1}{2} \rho ci^2\, \Omega^2 ri^2 \left[\left(\frac{yEA, i}{ci} - \frac{1}{4}\right) cL\alpha, i \cos\alpha i\, (\alpha i + \alpha q, i) + cD, i \sin\alpha i\right] \Delta ri\right]$$

Rotor pitching moment and rotor rolling moment are defined as follows :

$$LR = \sum_{1}^{NB} \int_{0}^{R} r sin\psi dT$$

$$MR = \sum_{1}^{NB} \int_{0}^{R} (-r\, cos\psi)\, dT$$

Blade aerodynamic forcing moments derived with the aid of analytical integration (i.e. homogeneous span-wise distributions of blade geometry and aerodynamic properties are assumed) are :

$$M\psi\,,A = \frac{1}{8}\rho c\Omega^2 R^4 [\, cL\alpha\, \varphi(\alpha + \frac{4}{3}\alpha q) - cD\,]$$

$$M\beta\,,A = \frac{1}{8}\rho c\Omega^2 R^4 [\, cL\alpha\, (\alpha + \frac{4}{3}\alpha q) + \varphi cD\,]$$

$$M\theta\,,A = \frac{1}{6}\rho\, c^2\Omega^2 R^3 [(\frac{yEA}{c} - \frac{1}{4})(cL\alpha\, (\alpha + \frac{3}{2}\alpha q)\cos\alpha + cD\sin\alpha) + cM\,]$$

the equations can be used in a simplified analytical model of auto rotating rotor blade aerodynamics and are also essential for linear stability analysis of rotor blades.

6. Blade Motion Computational Analysis

The mathematical structural blade model and the software is written by Bruno Zilli.
The finite element method represents a numerical method that is by far most popular in the field of structural dynamics and statics. Individual element matrices and the forcing vectors have to be assembled into the global matrices and the global forcing vector.

If time-marching simulation is used, structure global coordinates and their first time derivatives (i.e. deflections and rates) that were computed in the previous time step are used for calculation of corresponding accelerations.

If the system of equations of motion is linearized around the rotor speed, it can be written in a matrix form.

$$[M]\{q''\} + [C]\{q'\} + [K]\{q\} = [A]\{q'\} + [B]\{q\}$$

Here below is the software flow chart. Inria-Scilab has been chosen as a general developing platform because it's a free, well tested and open-source.
The software written by the author is available on this web page. **Anyone is welcome to try to modify, test or change the software in order to achieve better results.**

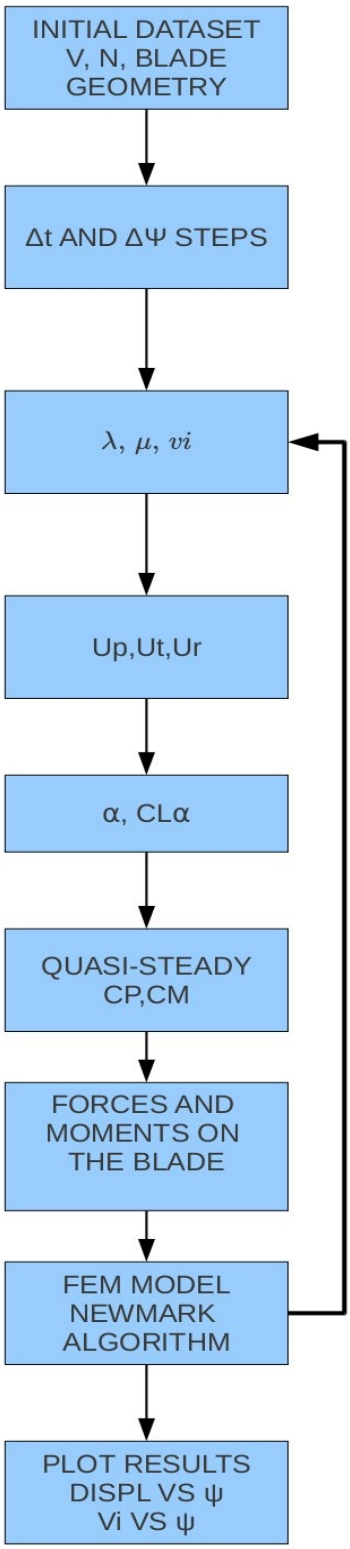
INITIAL DATASET
V, N, BLADE
GEOMETRY
Δt AND ΔΨ STEPS
λ, μ, vi
Up,Ut,Ur
α, CLα
QUASI-STEADY
CP,CM
FORCES AND
MOMENTS ON
THE BLADE
FEM MODEL
NEWMARK
ALGORITHM
PLOT RESULTS
DISPL VS ψ
Vi VS ψ

Here below are some results. A blade-flapping motion was simulated. The values are:
Blade length = 0,5 m
Blade rev speed = 290 rev/min
Autogyro weight = 10 N
Autogyro forward speed = 10 m/s
Blade profile = NACA 8H12
Blade materials = Balsa + 2 carb strips
Blade weight on the tip = 10 g
Blade flexible hinge at the root = polymer flexible hinge

An integration step of 0,001 s (integration step every 1,74° at 290 rev/min) has been used and the simulation for 90° of rotation, starting from 0° by the usual angle counting way (x axis).

The blade inertia values (carbon-balsa cross section) have been calculated by a fem analysis using code_aster, the EDF open source certified, powerful and free software. Files are available on this web page.

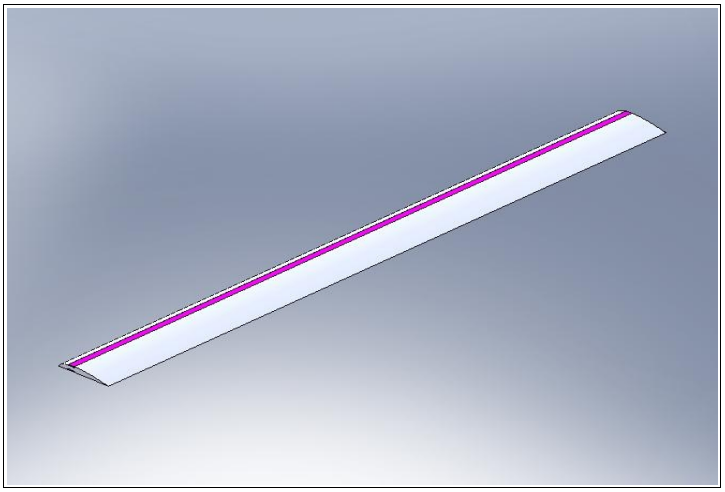

Blade general arrangement

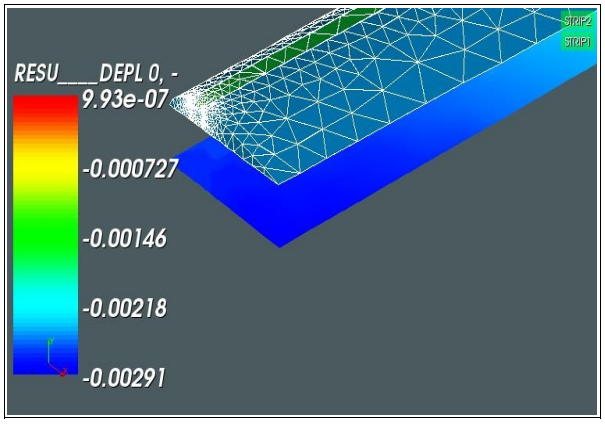

Blade fem analysis for cross section inertia values calculation

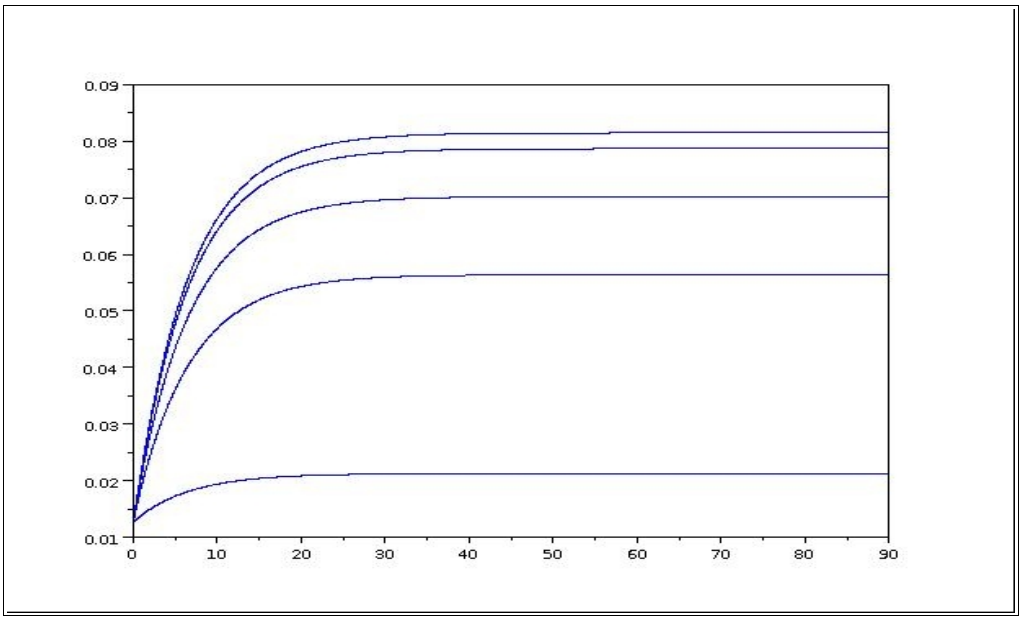

Blade motion for the first 90° starting by 0° (horizontal x-axis). The five curves are the positions of five points on the blade, by the increasing radial distance to the blade tip. The blade lifts by forwarding.

Here below is the induced inflow velocity. By using the right flexible hinge arrangement and a right sized flexible blade and weight, a good distribution of the induced inflow velocity has been obtained.

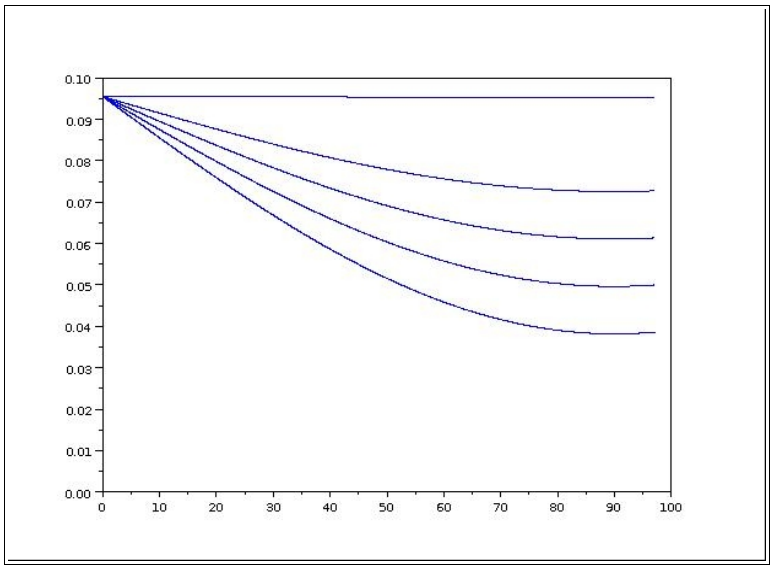

For a quick check of the results, the average coning angle b_0 obtained from the software results is:

$$b_0 = \arctan\left(\frac{0.083\,m}{0.5\,m}\right) = 9.42°$$

from an approximate usefully evaluation of the trusting and centrifugal forces, we have:

$$b_0 = \frac{\frac{10\,(N, weight)}{3\,(blades)}}{0.065\text{kg} * 30^2 * 0.25\text{m} + 0.01\text{kg} * 30^2 * 0.5\text{m}} = 9.87°$$

A difference of 5% approximatively is a good result for such kinds of applications.

7. Flapping Hinge Offset and Flexible Hinge-less Rotors

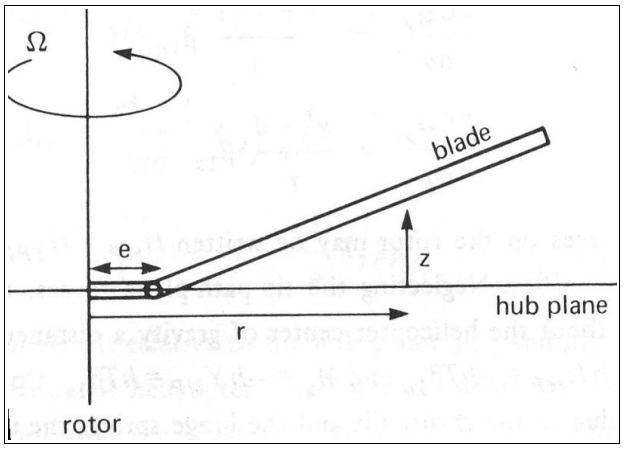

Consider an articulated rotor with the flap hinge offset from the center of rotation by a distance eR=0.04-0.05 R, as the figure above. It has a simpler mechanical construction than the other with no offset, and it has a favorable influence on the helicopter handling qualities, because it produces a flap pulsation above Ω . For a no hinge spring blade, the result is:

$$\Omega_e^{\,2} = \Omega^2\left[1 + \frac{e\, r_{CG}\, m_{blade}}{I_{blade}}\right]$$

Where r_{cg} is the blade CG distance from the hinge; m_{blade} is the blade mass. I_{blade} is the moment of inertia about the flap hinge. Typically $\Omega_e > \Omega$ about ν = 1.02-1.04 and this is good for increased rotor stability.

We're now introducing the lock number, that is: $\gamma = \frac{\rho a c R^4}{I_B}$

a is the airfoil lift curve slope, and ρ is the air density.

γ is a dimensionless parameter representing the ratio of aerodynamic forces to inertial forces. Typically γ ≈ 8-10 for articulated rotors.

Consider an articulated rotor blade with no hinge offset from the center of rotation, but now with a spring acting on the blade that produces a restoring moment of the blade itself.

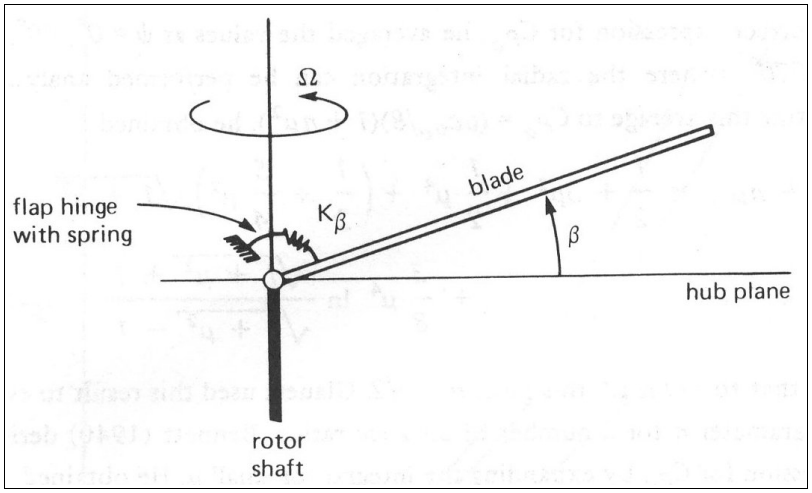

It is assumed that the blade motion still consists of only rigid rotation about the flap hinge, so that the out-of-plane deflection is z = rβ.

The spring stiffness which might be used on a rotor blade would be small compared to the centrifugal stiffening, however, so the rigid flapping assumption is reasonable. With rigid flapping motion, it follows that the equations for the rotor forces and power are unchanged. The hinge spring does change the rotor flapping motion, since it introduces an additional flap moment. Because the spring moment is proportional to the flapping displacement relative to the shaft, the hub plane is the appropriate reference plane in this case.

Being K_β [Nm] the spring rate and β_p the static angle, we assume the $K_\beta = 0$ for β_p. The flapping equation become:

$$I_b(\ddot{\beta}+\Omega^2\beta)+K_\beta(\beta-\beta_p)=\int rF_z\,dr$$

or

$$(\ddot{\beta}+\nu^2\beta)=(\nu^2-1)\beta_p+\int (r\frac{F_z}{ac})\,dr$$

The dimensionless natural flap frequency of the rotating frame is:

$$\nu^2=[1+\frac{K_\beta}{I_{blade}\Omega^2}]$$

For practical flap springs, ν will be just slightly greater than one. When ν>1, the aerodynamic forces acting at 1/rev (dimensionless Ω) are no longer forcing the flap motion exactly at resonance (ν=1).
Thus the rotor responds to this periodic excitation with a reduced magnitude and reduced phase proportional to:

$$\left[1+\left(\frac{\nu^2-1}{\frac{\gamma}{8}}\right)^{2\,(-1/2)}\right] \qquad \left[90-\tan^{-1}\left(\frac{\nu^2-1}{\frac{\gamma}{8}}\right)\right]$$

Increasing the flap frequency so that periodically the system is forced below resonance slightly reduces the amplitude of flap response to cyclic excitation, and most important reduces the lag in the response. For example, when ν = 1.15 and γ=8, the amplitude is reduced only about 5%, but the lag becomes 72° instead of 90° for an articulated rotor.

Example: how to build a flexible hub.

Here above on the left is a general scheme about a flexible hub invented by the soviets A. Tatarnikov and O. Polyntsev. The rotor consists of two blades attached to the hub, which incorporates three flapping hinges and flexible beams, restricting individual flapping of the blades. There's a general arrangement on the right.

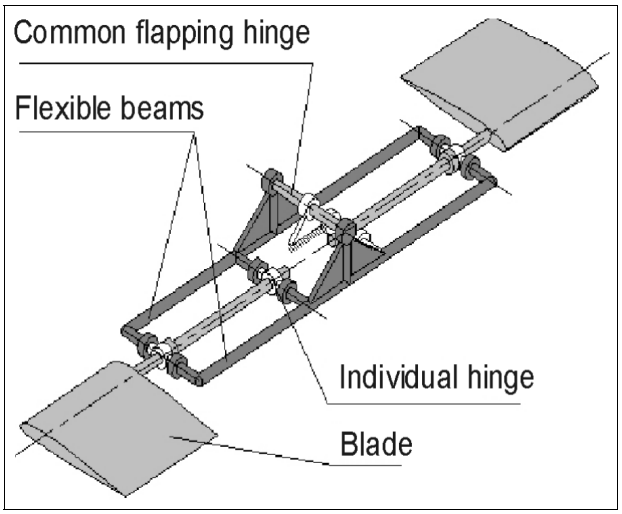

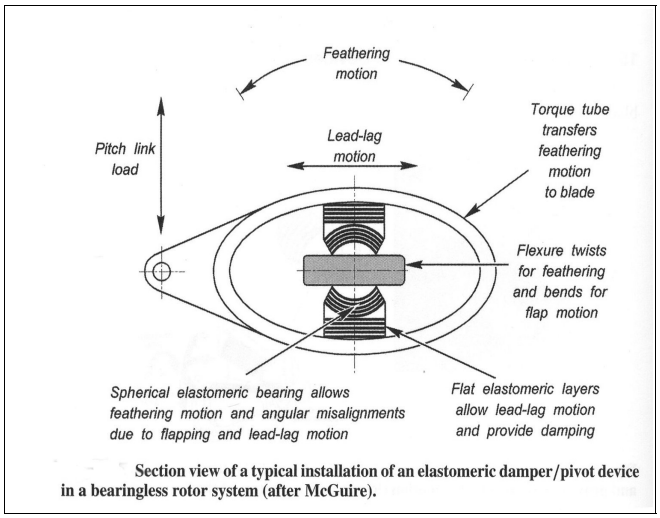

Section view of a typical installation of an elastomeric damper/pivot device in a bearingless rotor system (after McGuire).

Here below are some arrangements for a r.c. autogyro model flexible hub.

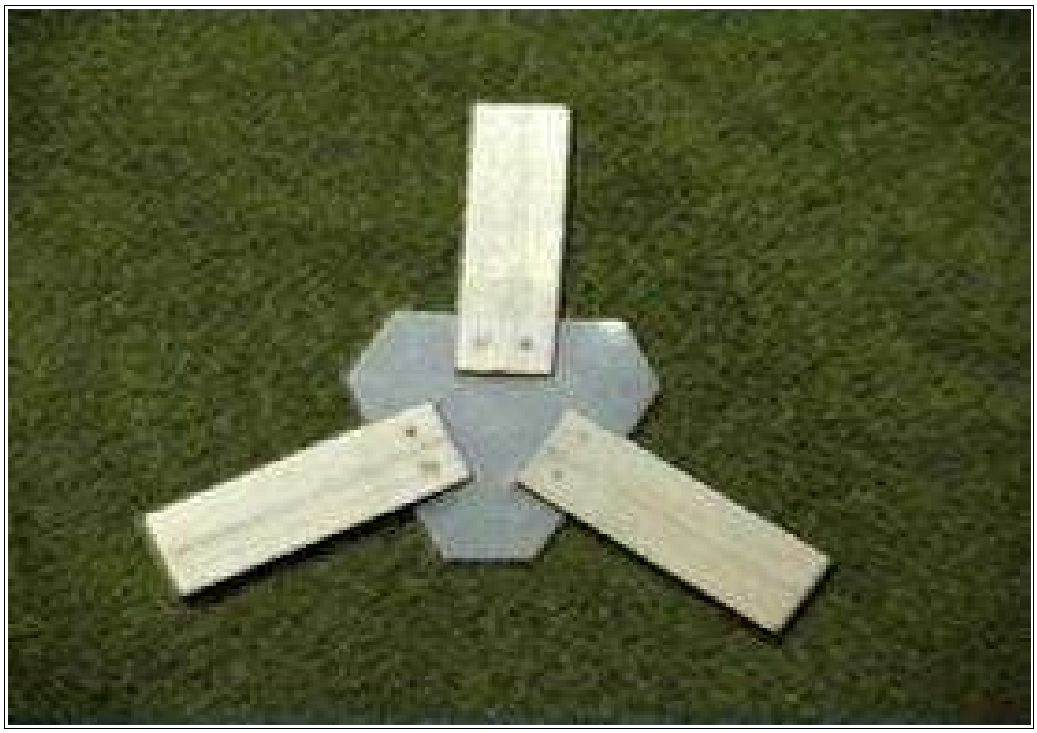

8. Delta Hub Rotor

Pitch-flap coupling is a kinematic feedback of the flapping displacement to the blade pitch motion, that may be described by $\Delta\theta = -K_p \beta$. For positive pitch-flap motion coupling ($K_p > 0$). flap up decreases the blade pitch and hence the blade angle of attack.
The resulting lift reduction produces a change in flap moments that opposes the original flap motion. Thus positive pitch-flap coupling acts as an aerodynamic spring on the flap motion. Pitch-flap coupling may be obtained entirely by mechanical means. The simplest approach is to skew the flap hinge by an angle universally called δ_3, so that it's no longer perpendicular to the radial axis of the blade.

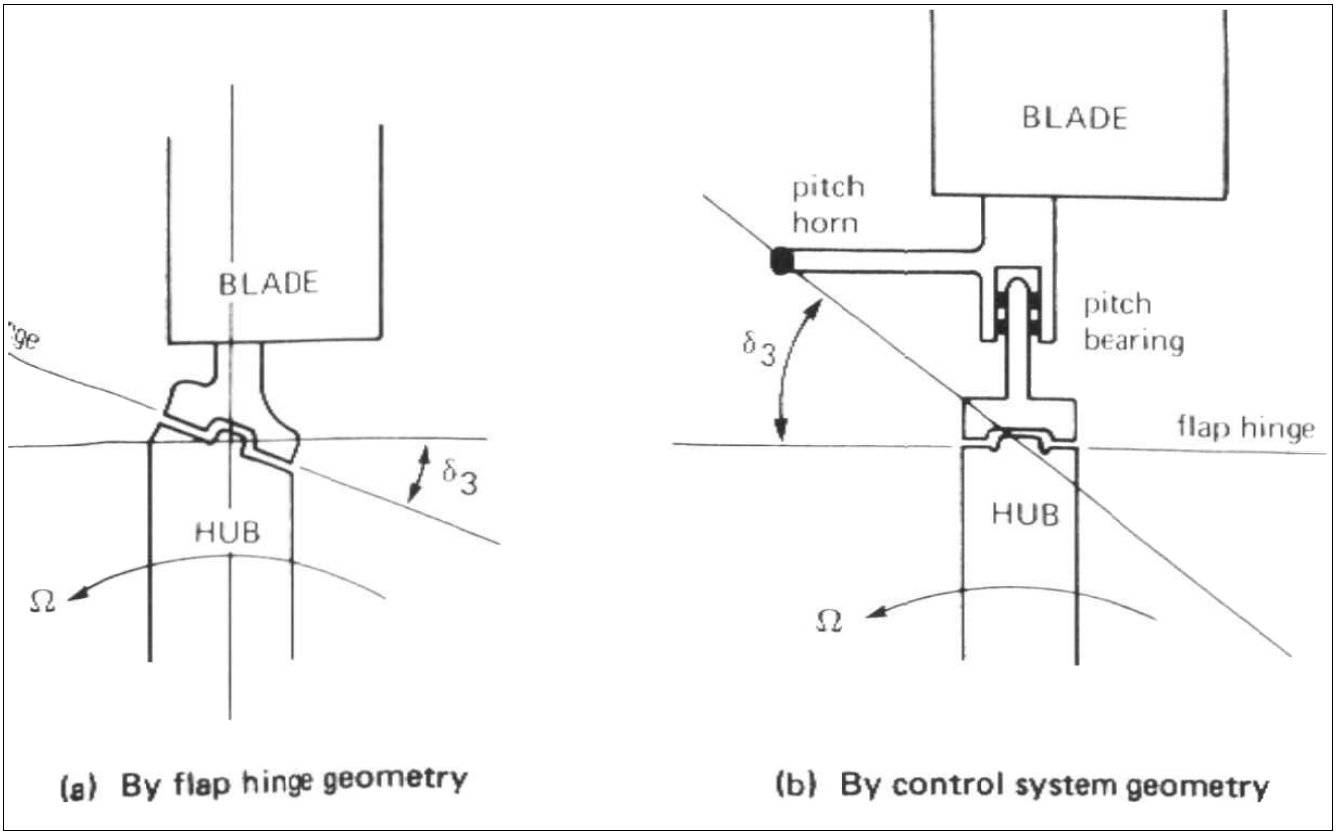

Then a rotation around the hinge with a flap angle β must also produce a pitch change of $-\beta \tan \delta_3$. The feedback gain for this arrangement is therefore $K_p = \tan \delta_3$. Pitch-flap coupling is usually defined in terms of the delta-three angle. Note that positive coupling $\delta_3 > 0$ represents negative feedback, decreasing the blade pitch for a flap increase. Pitch-flap coupling can also be introduced by the control system geometry. When the pitch bearing is outboard of the flap hinge, the blade will experience a pitch change due to flapping if the pitch link is not in line with with the axis of flap hinge.
For a fixed swash plate position, the flap motion can be viewed as occurring around a virtual hinge axis joining the end half the pitch horn and the actual flap hinge. The δ_3 angle then is the angle between this virtual hinge axis and the real flap hinge axis.

Thus pitch-flap coupling introduces an aerodynamic spring that increases the effective natural frequency of the flap motion to:

$$v_e^2 = [v^2 + \frac{\gamma}{8} K_p]$$

The magnitude and phase of the tip-path-plane response to cyclic becomes:

$$\frac{\beta}{\theta} = \frac{1}{\sqrt{1 + Kp^2}} \qquad \Delta\psi = 90° - \delta 3$$

Here below are some pictures of the delta hub construction.

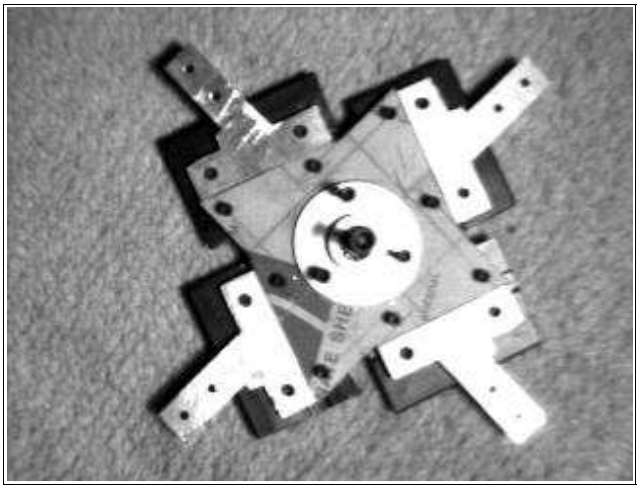

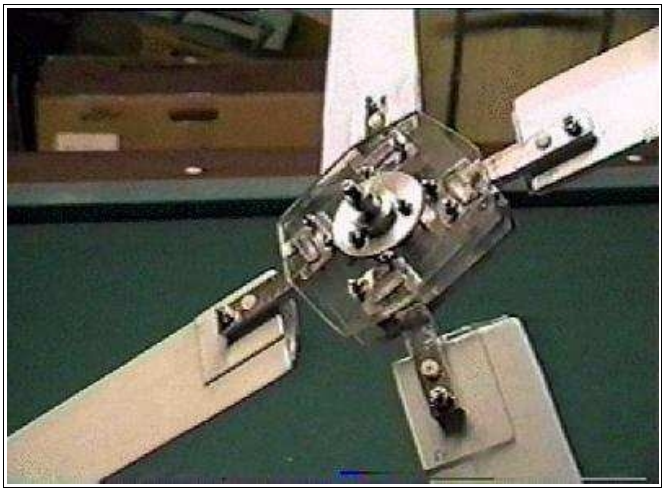

9. Rotor Stability

We analyze the rotor flutter stability in particular the pitch flap motion of the blade. The classical problem considers two degrees of freedom, the rigid flap and the rigid pitch of an articulated rotor blade. The rotation of the wing introduces a number of effects that make blade flutter much different from the fixed wing phenomenon.

We define M_F and M_f the aerodynamic flap and pitch moments;

$\gamma = \frac{\rho a c R^4}{I_B}$ the blade lock number;

$I_\beta = \int (\eta_\beta)^2 \, m dr$ where η_β is mode shape of fundamental flap model. For a hinge offset e, we have $\eta_\beta = \frac{r-e}{1-e}$ and normalized to 1 at the tip;

$I_b = \int m r^2 \, dr$ is the characteristic inertia of the rotor blade or the inertia flapping moment;

$I_\beta^\circ = \frac{I_\beta}{I_b}$

$I_x = \int x_I m r \, dr$ inertial flap-pitch coupling, and x_I the chordwise offset of blade center of gravity behind the pitch axis;

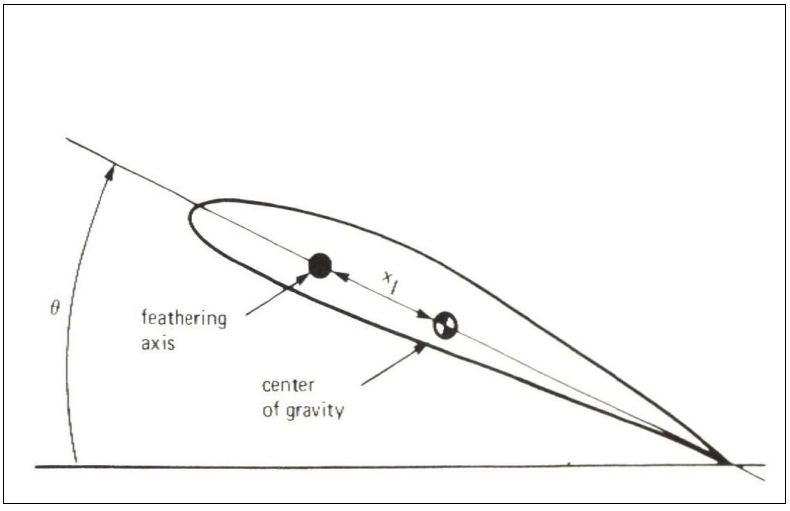

$I_f = \int I_\theta \, dr$ Blade pitch inertia, where I_θ is the section moment of inertia with respect to the feathering axis;

$$I_x^\circ = \frac{I_x}{I_b} \qquad I_f^\circ = \frac{I_f}{I_b}$$

I''_x , I''_f and I''_β are dimensionless quantities and the integrals are from 0 to 1.

The differential equation of the rigid flap and rigid pitch motion of a rotor blade are:

$$I_\beta^\circ(\ddot{\beta}+\nu_\beta{}^2\,\beta)-I_x^\circ(\ddot{\theta}+\theta)=\gamma M_F \qquad I_f^\circ\,[\ddot{\theta}+(\omega_\theta{}^2+1)\,\theta]-I_x^\circ\,(\ddot{\beta}+\beta)+K_P\,I_f^\circ\,\omega_\theta{}^2\,\beta=\gamma M_f$$

Here β is the degree of freedom of perturbation flap motion, with rotating natural frequency ν_β and θ is the pitch degree of freedom, with non rotating frequency ω_θ.

The flap moment M_F and the pitch moment M_f are expressed as coefficients (hovering). $C(k_e)$ is the wake lift deficiency function and we can set it as 1 for model tasks:

$$M_\theta=\frac{1}{8}\,C(k_e) \quad M_{\dot\theta}=\frac{c}{12}\,[\frac{1}{2}+C(k_e)(1+2\frac{x_A}{c})] \quad M_{\dot\beta}=\frac{-1}{8}\,C(k_e) \quad M_\beta=\frac{c}{12}\,C(k_e)(1+2\frac{x_A}{c})$$

$$m_\theta=\frac{-x_A}{6}\,C(k_e) \quad m_{\dot\theta}=\frac{-c^2}{32}\,[1+2\frac{x_A}{c}][1+4\frac{x_A}{c}\,C(k_e)] \quad m_{\dot\beta}=\frac{x_A}{6}\,C(k_e)$$

$$m_\beta=\frac{-c^2}{64}\,[1+8\frac{x_A}{c}\,C(k_e)(1+2\frac{x_A}{c})]$$

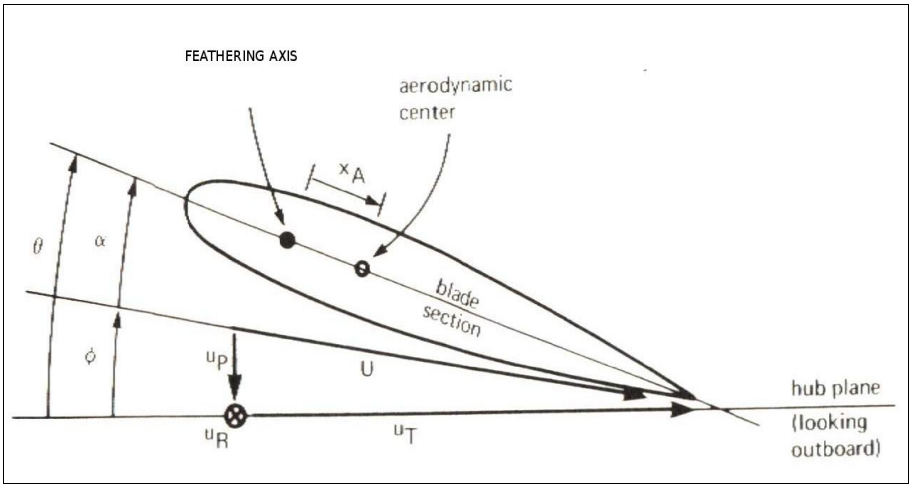

x_A is the distance the aerodynamic center is behind the feathering axis as visible above.

The coupled differential equations for the flap and pitch motion are thus:

$$\begin{bmatrix} I_\beta^\circ & -I_x^\circ \\ -I_x^\circ & I_\beta^\circ \end{bmatrix}\begin{Bmatrix} \ddot{\beta} \\ \ddot{\theta} \end{Bmatrix} + \begin{bmatrix} -\gamma M_{\dot\beta} & -\gamma M_{\dot\theta} \\ -\gamma m_{\dot\beta} & -\gamma m_{\dot\theta} \end{bmatrix}\begin{Bmatrix} \dot{\beta} \\ \dot{\theta} \end{Bmatrix} + \begin{bmatrix} I_\beta^\circ \nu_\beta^{\,2} - \gamma M_\beta & -I_x^\circ - \gamma M_\theta \\ -I_x^\circ + K_p\, I_f^\circ \omega_\theta^2 - \gamma m_\beta & I_f^\circ(\omega_\theta^2+1) - \gamma m_\theta \end{bmatrix}\begin{Bmatrix} \beta \\ \theta \end{Bmatrix} = 0$$

In hovering the aerodynamic coefficients are constants, no forcing terms are considered for the stability analysis. In Laplace domain ($s=\alpha+i\omega$) we have:

$$[A]\begin{Bmatrix} \beta \\ \theta \end{Bmatrix} = \begin{bmatrix} I_\beta^\circ s^2 - \gamma M_{\dot\beta} s + I_\beta^\circ \nu_\beta^{\,2} - \gamma M_\beta & -I_x^\circ s^2 - \gamma M_{\dot\theta} s - I_x^\circ - \gamma M_\theta \\ -I_x^\circ s^2 - \gamma m_{\dot\beta} - I_x^\circ + K_p\, I_f^\circ \omega_\theta^2 - \gamma m_\beta & I_f^\circ s^2 - \gamma m_{\dot\theta} s\, I_f^\circ(\omega_\theta^2+1) - \gamma m_\theta \end{bmatrix}\begin{Bmatrix} \beta \\ \theta \end{Bmatrix} = 0$$

The eigenvalues are the roots ω_θ of the characteristic equation det [A] = 0. A plane of the system parameters has regions in which all the roots have negative real parts, so that the motion is stable; and regions in which one or more roots have positive real parts, so that the motion is unstable. There are two ways a root can cross the imaginary axis into the right half plane, producing an unstable system: as a real root along the real axis, and as a complex conjugate pair at finite frequency.
The instability associated with the real root going through the origin into the right half plane is called divergence. It's a static instability, since with zero frequency no velocity or acceleration forces are involved. **The instability associated with a complex conjugate pair of roots crossing the imaginary axis is called flutter. This instability involves an oscillatory motion of the system.**

The motion significant parameters for the rotor blade flutter stability are the pitch natural frequency ω_θ, determined by the system stiffness; and offsets of the center of gravity and aerodynamic center from the reaction axis.

The separation of the center of gravity and aerodynamic center ($x_I - x_A$) is more important than their distance from the reaction axis, but x_A must be kept small to avoid large oscillatory loads in forward flight. Typically $x_A = 0$. Thus the principal parameters controlling the blade flutter stability are the pitch stiffness (ω_θ) and the chordwise mass balance (x_I).

Using $I_x^\circ \approx \frac{3}{2} x_I$ the condition for avoiding the static divergence is:

$$x_I - \frac{8\nu_\beta^{\,2}}{9}\, x_A < \frac{16}{3\gamma}\, \nu_\beta^{\,2}\, I_f^\circ\, (\omega_\theta^2+1) + \frac{\gamma c^2}{96} + \frac{2}{3}\, K_p\, I_f^\circ\, \omega_\theta^2$$

which shows that the divergence depends on the distance the center of gravity is aft of the aerodynamic center ($x_I - x_A$). The boundary is relatively insensitive to the pitch axis (reaction) location for a fixed ($x_I - x_A$), even $x_A = 0$ is commonly used . **Having ($x_I - x_A$) < 0 by setting the blade center of gravity ahead the aerodynamic center is a condition for the assured divergence stability, regardless of pitch stiffness (ω_θ).**

A flutter instability occurs when a pair of complex conjugate roots cross the imaginary axis into the right plane. The flutter stability boundary is thus defined by the requirement that the one root is on the imaginary axis, s=iω, where ω is a real and positive frequency.
On substituting s=iω in the characteristic equation det [A] = 0, we obtain two equations (Re and Im). Eliminating ω^2 from the two equations we have a single relation defining the flutter boundary in terms of blade parameters. The criterion for flutter stability can be written as:

$$\omega_\theta^4 + A\,\omega_\theta^2\,\frac{I_x}{I_f} + B\,\omega_\theta^2 + C\,\frac{I_x}{I_f} + D > 0$$

On the plane ω_θ^2 vs. I_x/I_f the flutter stability boundary is a hyperbola.

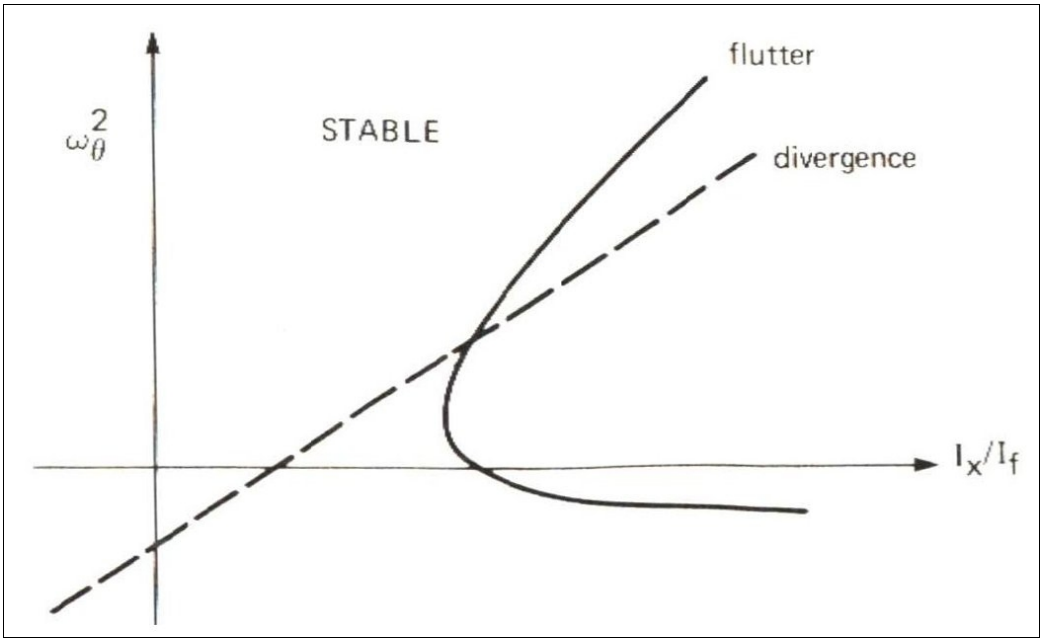

The minimum I°_x on the flutter hyperbola occurs at:

$$\frac{I_x}{I_f} = \frac{-2\sqrt{D} - B}{A}$$

With articulated rotors, and $I^\circ_x \approx (3/2)\, x_I$ it is:

$$x_I - \frac{8}{9}\,x_A = c^2\left(\frac{1}{3\sqrt{2}} + \frac{\gamma}{48}\right)$$

Consequently, if the blade is mass balanced in such a way that the center of gravity is no farther aft than this distance, flutter stability is assured regardless of the pitch stiffness (ω_θ).

10. Vehicle stability

In this chapter a study is reported on the model longitudinal stability by investigating the equations of motion. The balance momentum and angular momentum equations have been written in the model CG.

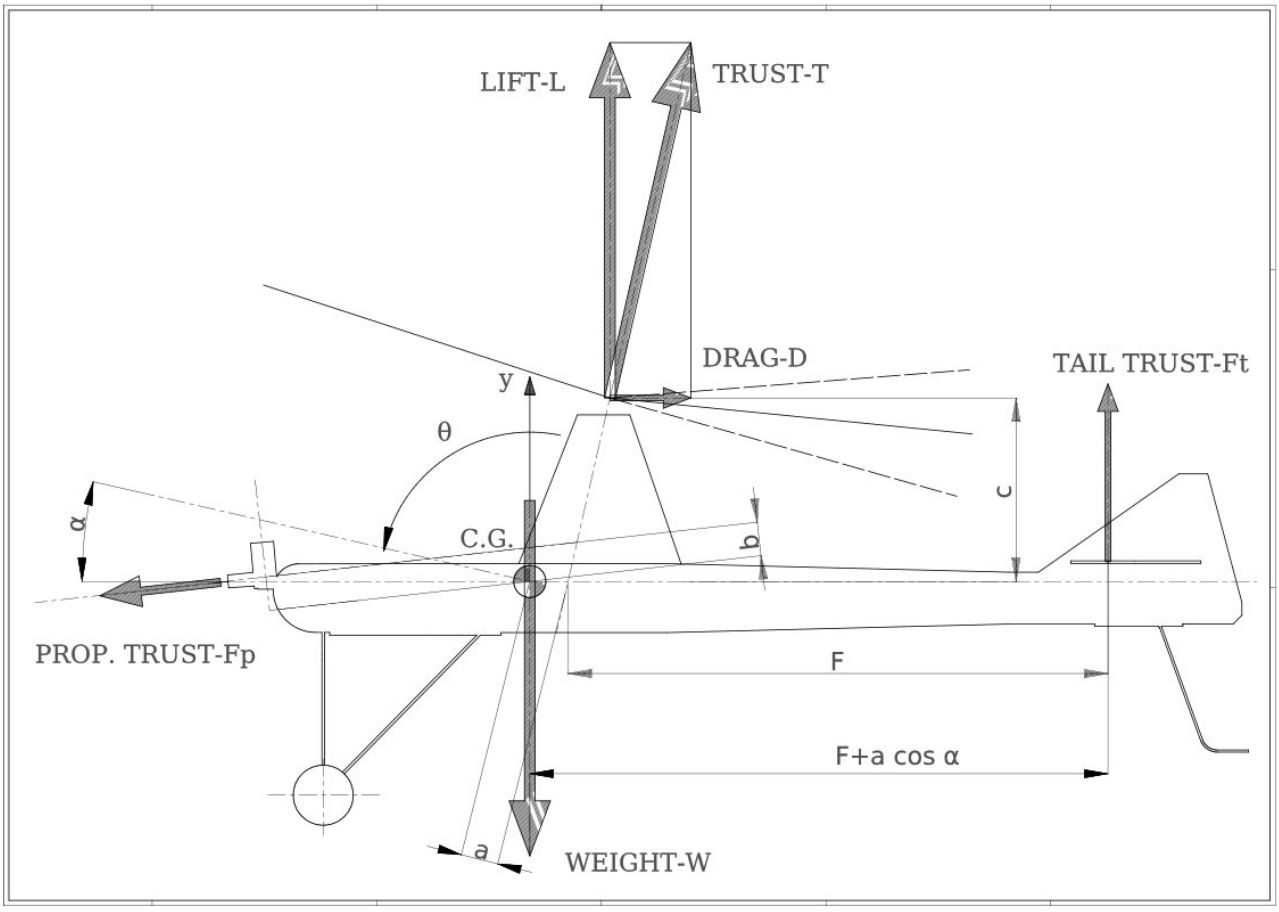

In particular, for the pitch degree of freedom θ the angular momentum balance equation written on the model center of mass gives (cos α ≈ 1) :

$$I_m\ddot{\theta}=T(\theta)a-D(\theta)c-F_t(\theta)(a+F)+F_p b$$

For θ increasing from zero, F_t is downward because the tail profile is a simple plate. So it's the sign minus sign in the angular momentum balance equation.

by using the Glauert's theory, it is:

$$I_m\ddot{\theta}=[\frac{1}{3}\sigma kL\theta](\pi R^2\rho\Omega^2R^2)a-\delta(\pi R^2\rho\Omega^2R^2)c-F_t(\theta)(a+F)+F_p b$$

F_t is the tail total circulatory lift plus the so called added mass effect (ρ is the air density). Simplifying for model tasks it is:

$$F_t(\theta,\dot{\theta},\dot{y},\ddot{y})=\frac{1}{2}\rho U^2 S_t[2\pi(\theta(t)+\frac{\dot{y}(t)}{U}+\frac{(a+F)\dot{\theta}(t)}{U})]+(\pi\rho(\frac{c}{2})^2 l_t)\ddot{y}(t)$$

U is the model horizontal speed, S_t is the tail surface and l_t the tail length. The tail chord c has been considered as constant.

The momentum balance equation written on the model C.G. is:

$$m\ddot{y}(t)=L-W+F_t$$

by using the Glauert's theory, and for small angles of rotor incidence, we have:

$$m\ddot{y}(t)=[\frac{1}{3}\sigma kL\theta](\pi R^2\rho\Omega^2R^2)-W-\frac{1}{2}\rho U^2 S_t[2\pi(\theta(t)+\frac{\dot{y}(t)}{U}+\frac{(a+F)\dot{\theta}(t)}{U})]+(\pi\rho(\frac{c}{2})^2 l_t)\ddot{y}(t)$$

It is more useful organizing the equations in a matrix form:

$$\begin{bmatrix} m-(\pi\rho(\frac{c}{2})^2 l_t) & 0 \\ I_m & (\pi\rho(\frac{c}{2})^2 l_t)(a+F) \end{bmatrix}\begin{bmatrix}\ddot{y}\\ \ddot{\theta}\end{bmatrix}+\begin{bmatrix} \frac{1}{2}\rho U S_t & \frac{1}{2}\rho U S_t(a+F) \\ \frac{1}{2}\rho U S_t(a+F) & \frac{1}{2}\rho U S_t(a+F)^2 \end{bmatrix}\begin{bmatrix}\dot{y}\\ \dot{\theta}\end{bmatrix}$$
$$+\begin{bmatrix} 0 & \pi\rho U^2 S_t-(\frac{1}{3}\sigma kL)(\pi R^2\rho\Omega^2R^2) \\ 0 & \pi\rho U^2 S_t(a+F)-(\frac{1}{3}\sigma kL)(\pi R^2\rho\Omega^2R^2)a \end{bmatrix}\begin{bmatrix} y\\ \theta\end{bmatrix}=\begin{bmatrix} -W \\ F_p b-\delta(\pi R^2\rho\Omega^2R^2)c \end{bmatrix}$$

For the stability analysis it's useful considering the equations without forcing terms. The solutions are in the form :

$$y(t)=y_0e^{(st)} \qquad \theta(t)=\theta_0e^{(st)}$$

where s = =α+iω are complex numbers.

By substituting the general solutions in the motion equations, simplifying and equating to zero, or directly doing the equations L-transformation, it is :

$$s^2\begin{bmatrix} m-(\pi\rho(\frac{c}{2})^2 l_t) & 0 \\ I_m & (\pi\rho(\frac{c}{2})^2 l_t)(a+F) \end{bmatrix}\begin{bmatrix} y_0 \\ \theta_0 \end{bmatrix} + s\begin{bmatrix} \frac{1}{2}\rho U S_t & \frac{1}{2}\rho U S_t(a+F) \\ \frac{1}{2}\rho U S_t(a+F) & \frac{1}{2}\rho U S_t(a+F)^2 \end{bmatrix}\begin{bmatrix} y_0 \\ \theta_0 \end{bmatrix}$$
$$+\begin{bmatrix} 0 & \pi\rho U^2 S_t-(\frac{1}{3}\sigma kL)(\pi R^2\rho\Omega^2 R^2) \\ 0 & \pi\rho U^2 S_t(a+F)-(\frac{1}{3}\sigma kL)(\pi R^2\rho\Omega^2 R^2)a \end{bmatrix}\begin{bmatrix} y_0 \\ \theta_0 \end{bmatrix}=\begin{bmatrix} 0 \\ 0 \end{bmatrix}$$

So it has non trivial solutions by equating to zero the determinant and finding s:

$$\begin{vmatrix} (m-(\pi\rho(\frac{c}{2})^2 l_t))s^2+s(\frac{1}{2}\rho U S_t) & s(\frac{1}{2}\rho U S_t(a+F))+\pi\rho U^2 S_t-(\frac{1}{3}\sigma kL)(\pi R^2\rho\Omega^2 R^2) \\ s^2 I_m+s\frac{1}{2}\rho U S_t(a+F) & s^2(\pi\rho(\frac{c}{2})^2 l_t)(a+F)+s(\frac{1}{2}\rho U S_t(a+F)^2)+\pi\rho U^2 S_t(a+F)-(\frac{1}{3}\sigma kL)(\pi R^2\rho\Omega^2 R^2)a \end{vmatrix}$$

By the use of Scilab-Inria, are calculated the s-polynomial roots. This second software written by the author is very simple, because Scilab has already been organized for such kind of task.

After a first trial, the eigenvalues calculated are:

lambda_#1	=	0	(it's a semi-definite system)
lambda_#2	=	- 0.0480716	(non periodic motion)
lambda_#3	=	- 18.080609 + 54.358677i	(damped vibration)
lambda_#4	=	- 18.080609 - 54.358677i	(damped vibration)

The real parts of the complex ones are negative, so the vehicle is stable with the tail action. The fact that if the tail surface is very small is intresting (just for a trial set it as 0.005 m^2), the real parts of the complexes ones become very close to zero. The autogyro needs a tail!

W I T H M O D E R N PHILADELPHIA FOR A B A C K G R O U N D AN A U T O G I R O OVER THE M I D - T O W N SECTION - 1930

TWO AUTOGIROS OVER LOWER M A N H A T T A N, NEW YORK 1930

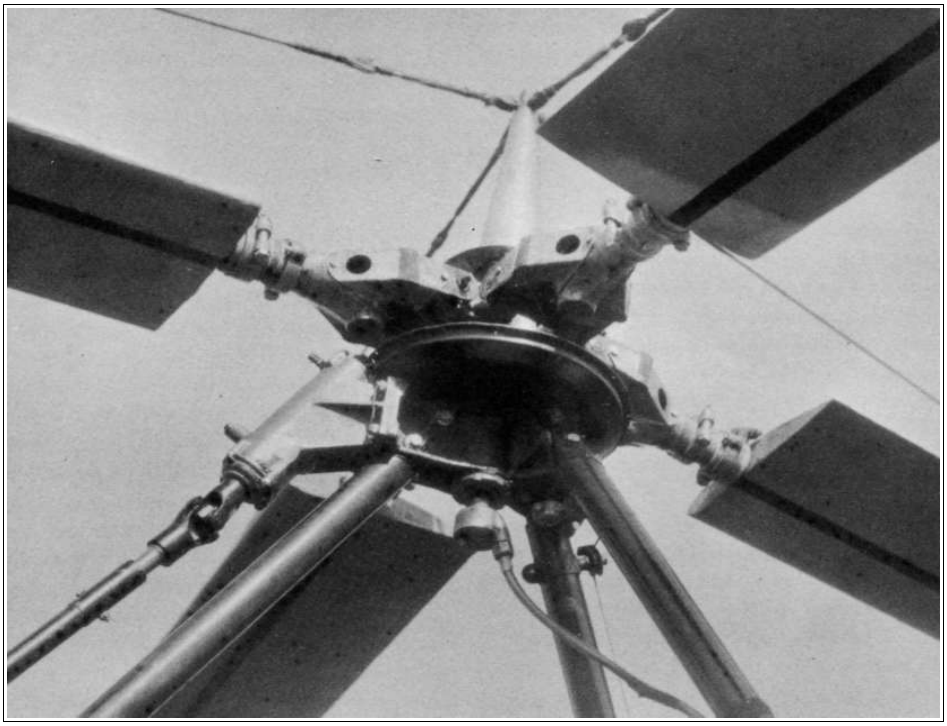

A CLOSE-UP OF THE AUTOGIRO ROTOR HEAD

JUAN DE LA CIERVA, INVENTOR OF THE AUTOGIRO.

A1. Bibliography and web sources

[1]-A General Theory Of The Autogyro-H. Glauert-1926

[2]-Principles of Helicopter Aerodynamics - J.G. Leishman - Cambridge – ISBN-978-0-521-85860-1

[3]-Aerodynamics Of The Helicopter – A. Gessow and G.C. Myers – ISBN – 0-8044-4275-4

[4]-Modern Gyroplane Design-Martin Hollmann-Aircraft Designs Inc. 25380 Boots Rd. -Monterey CA

[5]-Aeroelastic Modelling Of Gyroplane Rotors-J. Thralick-Ph.D. Thesis-Univ. Of Glasgow-UK

[6]-Helicopter Theory - Wayne Johnson - Dover - ISBN-0-486-68230-7

[7]-Rotary Wing Structural Dynamics And Aeroelasticity - R.L. Bielawa - AIAA-ISBN-1-56347-698-3

[8]-Bramwell's Helicopter Dynamics - G. Done and D. Balmford - AIAA – ISBN-1-56347-500-6

[9]-Rotary Wings Aerodynamics-W.Z. Stepniewski and C.N. Keys – Dover – ISBN 0-486-64647-5

[10]-Theory of Matrix Structural Analysis – J.S. Przemieniecky – Dover – ISBN – 0-486-64948-2

[11]-Aeroelasticity-Lectures-G. Dimitriadis-Université de Liège

[12]-Int. to Aircraft Aeroelasticity and Loads-J. Wright and J. Cooper-Wiley-ISBN-978-0470-85840-0

[13]-Mechanical Vibrations – Singiresu S. Rao – Addison Wesley – ISBN – 0-201-06550-9

[14]-Mod. and Sim. in Scilab/Scicos-Campell Cancellier Nikoukah-Springer-SBN-10: 0-387-27802-8

[15]-Matrix Struc. An. of Plane Frames using Scilab -Satish Annigeri -College of Eng. & Tech., Hubli

[16]-Scilab A Hands on Introduction-Satish Annigeri -College of Eng. & Tech., Hubli